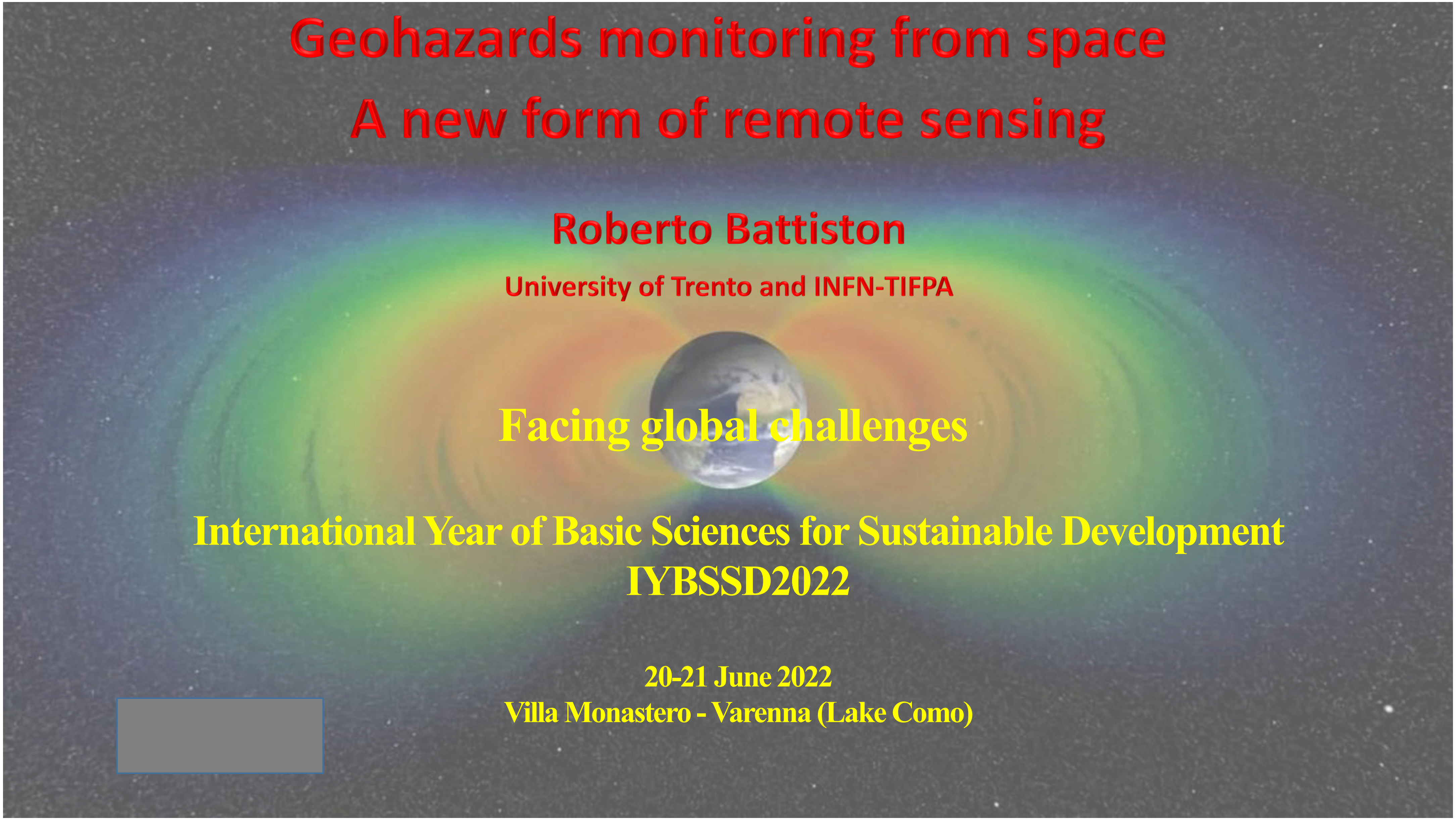
Geohazards monitoring from space
A new form of remote sensing
Roberto Battiston
University of Trento and INFN-TIFPA
Facing global challenges
International Year of Basic Sciences for Sustainable Development
IYBSSD2022
20-21 June 2022
Villa Monastero - Varenna (Lake Como)

LITHOSPHERE-ATMOSPHERE-IONOSPHERE-MAGNETOSPHERE COUPLING: A NEW KIND OF REMOTE SENSING FROM SPACE

Space is a privileged point of observation of the Earth.

Satellites and satellite constellations provide remote sensing, monitoring many physical variables at ground level, within the atmosphere, within the ionosphere and the magnetosphere.

It would be interesting to exploit space remote sensing to monitor seismic phenomena.

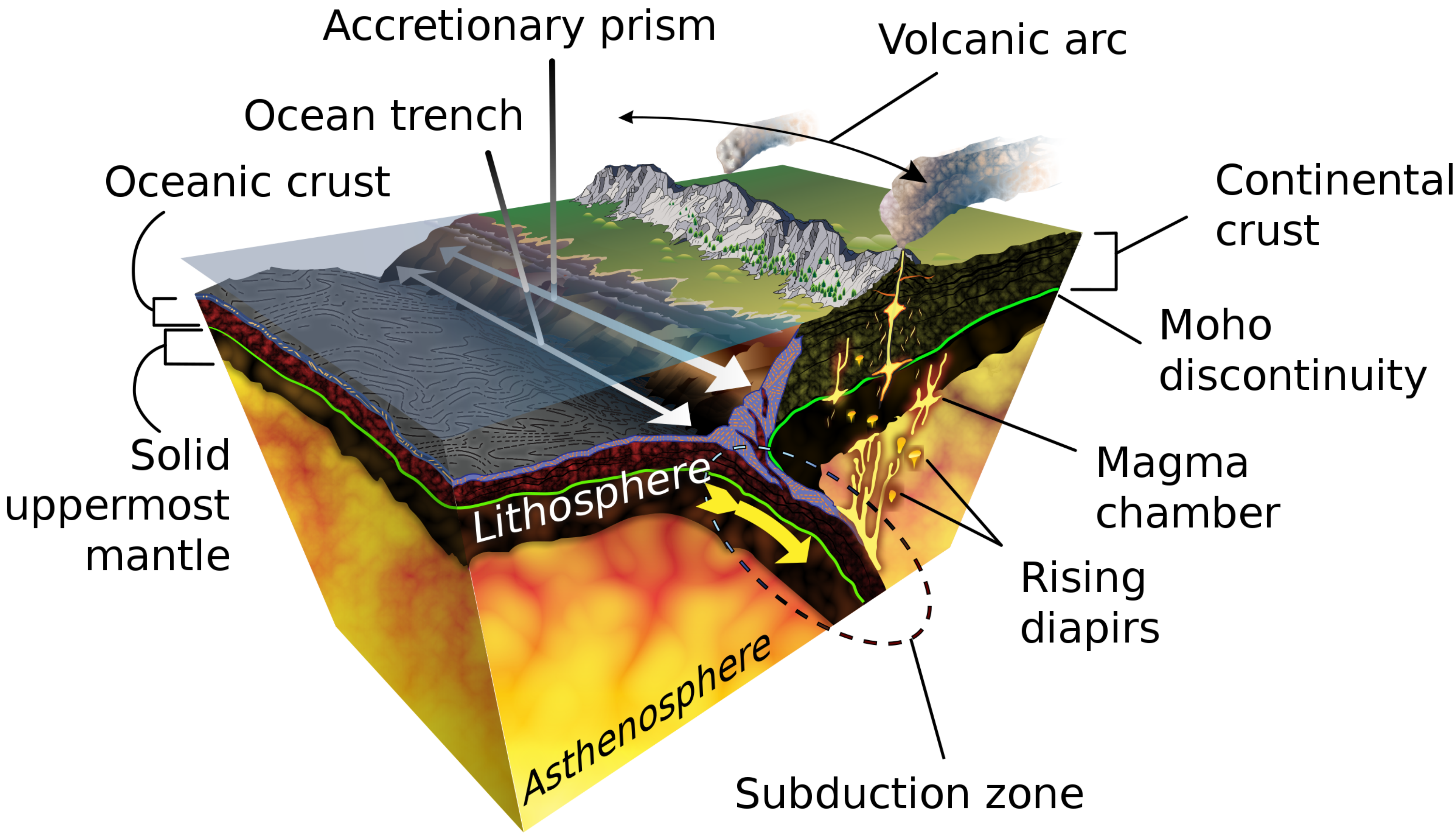
Accretionary prism
Volcanic arc
Ocean trench
Oceanic crust
Continental crust
Moho discontinuity
Solid uppermost mantle
Lithosphere
Magma chamber
Rising diapirs
Asthenosphere
Subduction zone

There is an ample literature discussing physical effects which could couple the lithosphere with the layers surrounding the Earth (atmosphere, ionosphere, magnetosphere)

However, many of the effects reported are of statistical nature

Other have been identified through the analysis of each given EQ

There is a general need of <u>causal</u> description of the coupling mechanisms

Real data on ground→numerical calculation to space

2011 M9.1 Tohuku-Oki (tsunami)

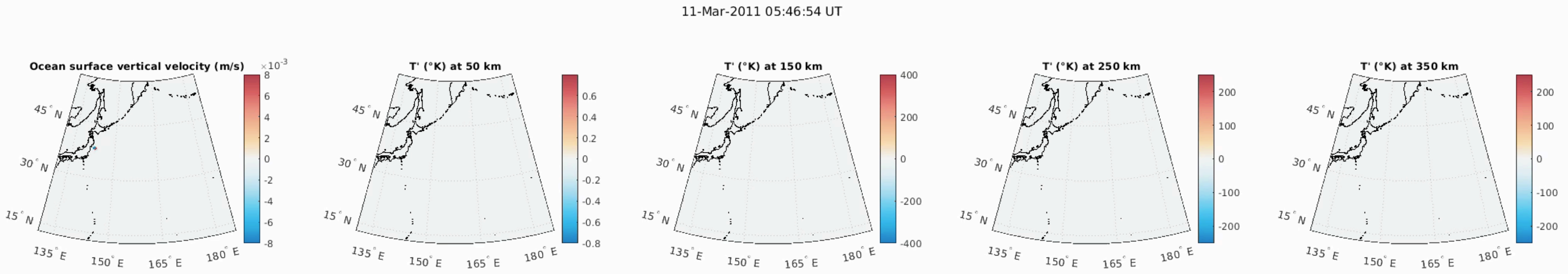

Inchin, et al. *, 2020*

2011 M9.1 Tohuku-Oki (tsunami)

Real data on ground→numerical calculation to space

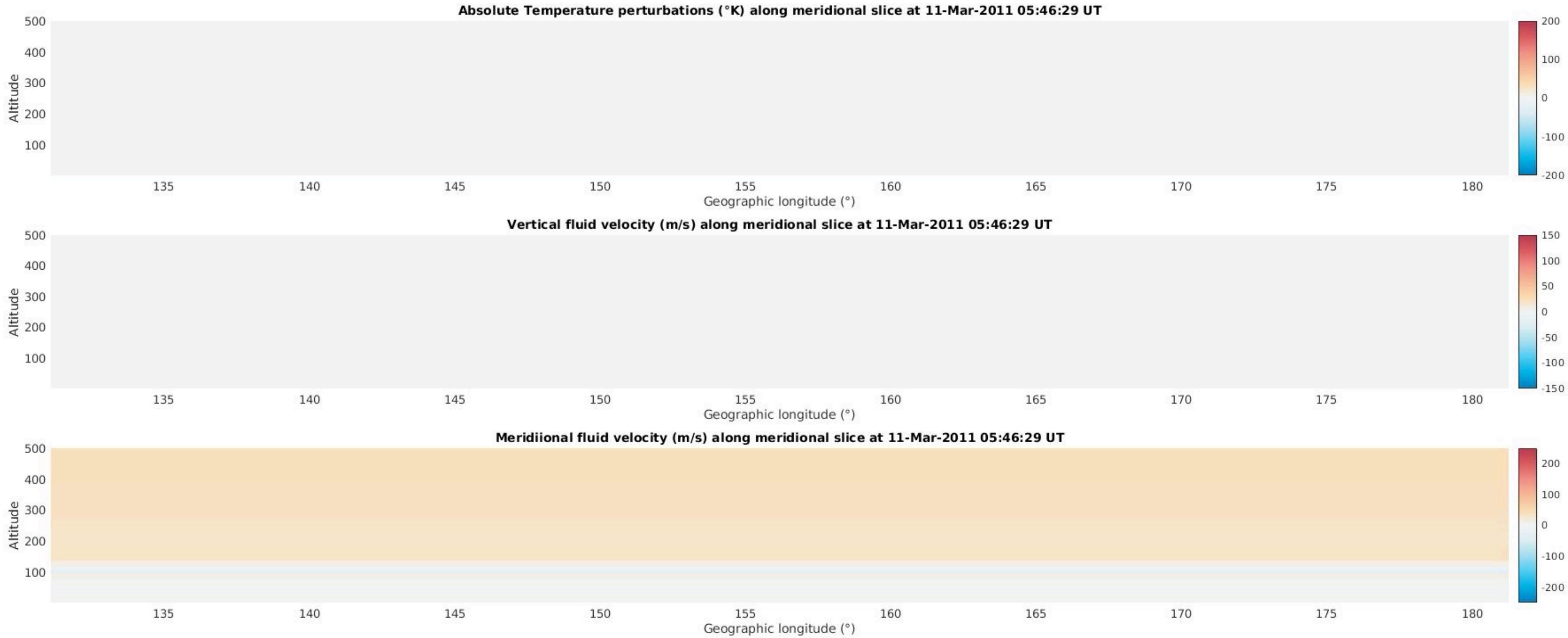

Inchin et al., *2020*

2016 M7.8 Kaikoura (earthquake)

Real data on ground→numerical calculation to space

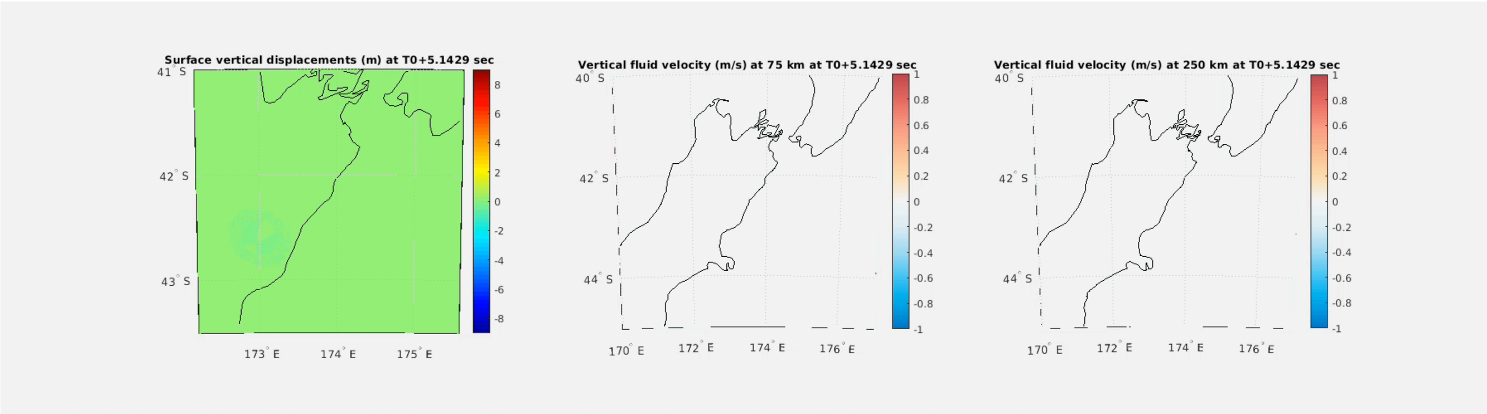

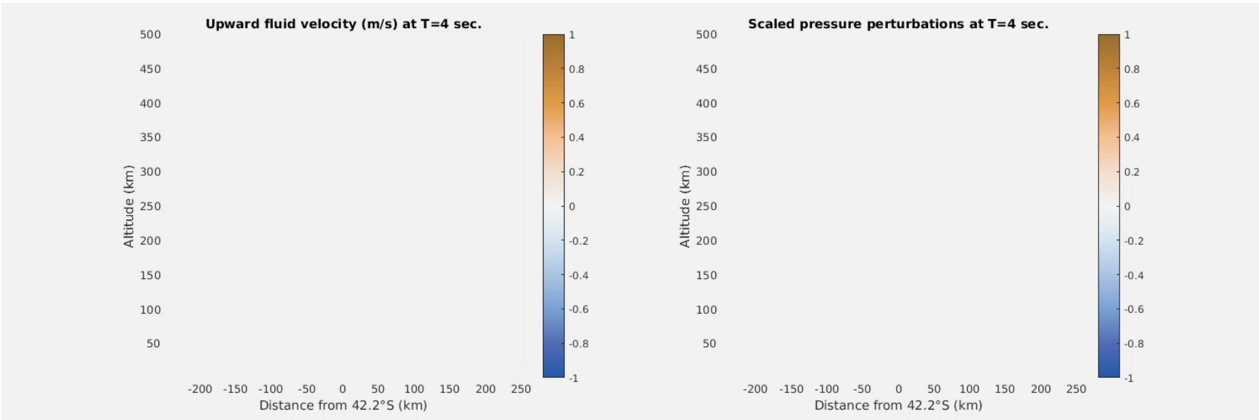

Inchin, et al., 2021

How to measure these coupling phenomena reliably ?

"If you want to find the secret of the universe, think in terms of energy, frequency and vibration"

Nikola Tesla

Atmospheric, Ionospheric Magnetospheric Invariants

A-I-M-I

The Earth and its surrounding layers host a huge amount of complex, interacting physical phenomena

In order to extract a clean set of <u>deterministic signals</u> exploiting <u>resonant or oscillating phenomena will provide a clear advantage</u>

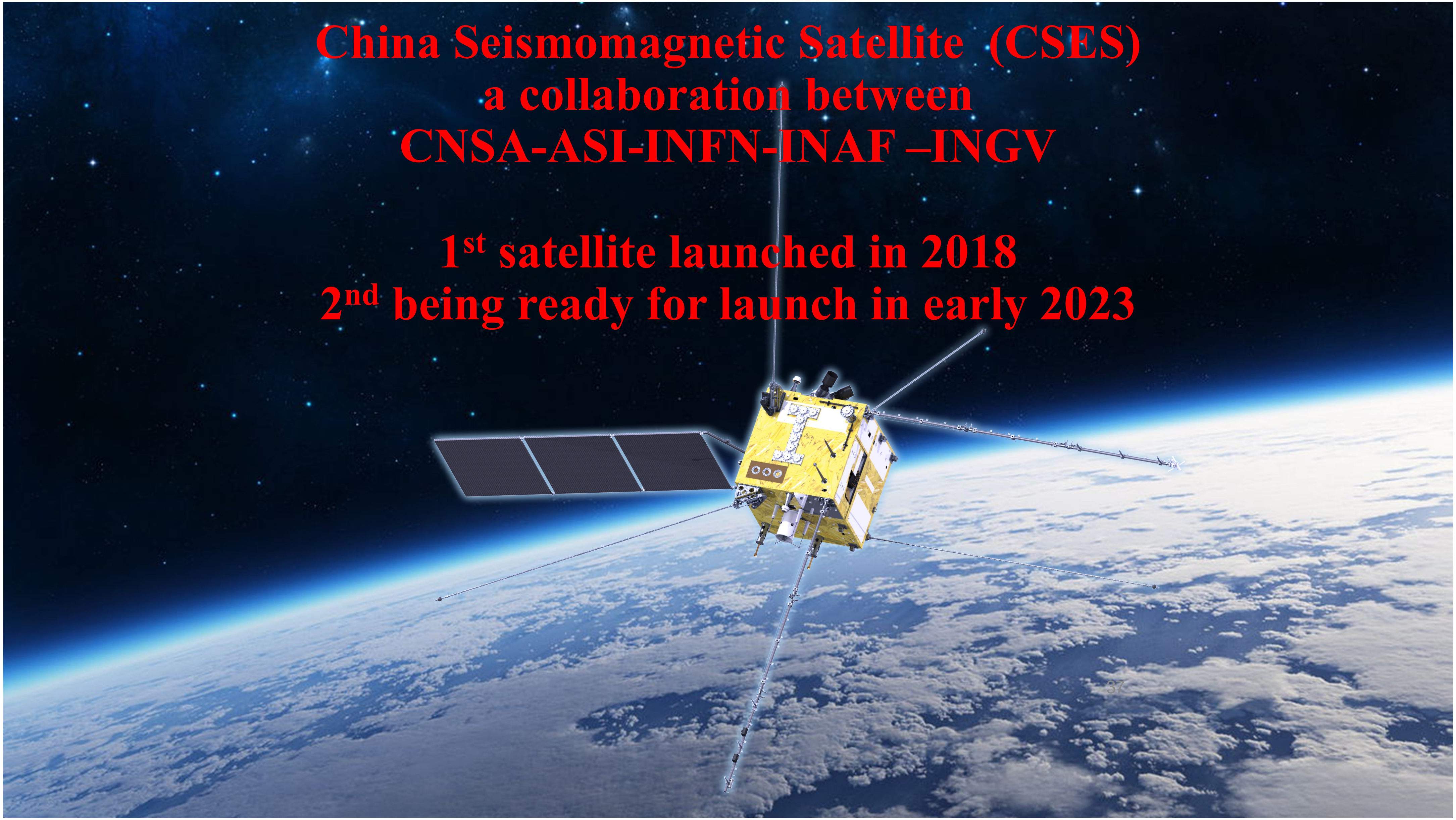
China Seismomagnetic Satellite (CSES)
a collaboration between
CNSA-ASI-INFN-INAF –INGV
1st satellite launched in 2018
2nd being ready for launch in early 2023

The LIMADOU collaboration

LIMADOU 利瑪竇

agenzia spaziale italiana

INFN
Istituto Nazionale di Fisica Nucleare

ISTITUTO NAZIONALE DI ASTROFISICA INAF
iaps

ISTITUTO NAZIONALE DI GEOFISICA E VULCANOLOGIA

Università di Roma Tor Vergata

UNIVERSITAS ATHESINA STUDIORUM

ALMA MATER STUDIORUM UNIVERSITÀ DI BOLOGNA A.D. 1088

UNINETTUNO

The status of Scientific Payloads on board CSES01

Payloads	Parameters	Status
High Precision Magnetometer (HPM) Two flux gate + one coupled dark state magnetometer (CDSM)	: DC to 16 Hz	Good health condition Excellent performance
Search-Coil Magnetometer (SCM)	10 Hz ~20 kHz	Good health condition and performance
Electric field detector (EFD)	DC~3.5 MHz	ULF/ELF/VLF good,
Plasma analyzer package（PAP)	Ion density : 10^2~10^7 cm^{-3} Ion temperature: 500~10000 K Ion content: H^+、He^+、O^+ Ion drift velocity: Vxyz	
Langmuir probe (LAP)	Electron density：1 0^2~$10^7 cm^{-3}$ Electron temperature： 500~10000K	Good health condition and performance
GNSS Occultation Receiver (GOR)	TEC、Ne Profile Air Refraction index, Profile of air temperature and pressure Ionospheric scintillation index	Good health condition and performance
Tri-Band Beacon (TBB) : Three bands：50/400/1066MHz		400 MHz band data processing algorithm and ground receivers not finished
Energetic particle detector (HEPP-H, L, X ray)	Proton flux：1.5MeV ~ 200MeV Electron flux： ≥100keV Pitch angle ： 5 ° HEPP-X : 0.9- 35 keV	Good health condition and performance
Italian Energetic particle detector (HEPD)	Proton flux: 30- 100 MeV Electron : 30 – 200 Mev ；	Good health condition and

LOCAL vs GLOBAL observables

Most effects connected to EQ's can be observed from space only when the satellite is orbiting over the EQ formation area

Some, like anomalies in the VAB particle fluxes or emission of EM waves, do propagate from the EQ formation area and can be observed at large distances

LOCAL OBSERVABLES

- Acoustic Gravity Waves (AGW)
- Frequency Line Resonances (FLR)
- Total Electron Content (TEC)
- ULF Electromagnetic Waves
- Plasma Density Waves (PDW)

GLOBAL OBSERVABLES

- VLF Electromagnetic Waves
- Van Allen Belt (VAB) electrons burst
- Schuman resonances

The MILC model is based on a set of deterministic signals exploiting resonant or oscillating phenomena

The MILC model – Piersanti et al.[2020]

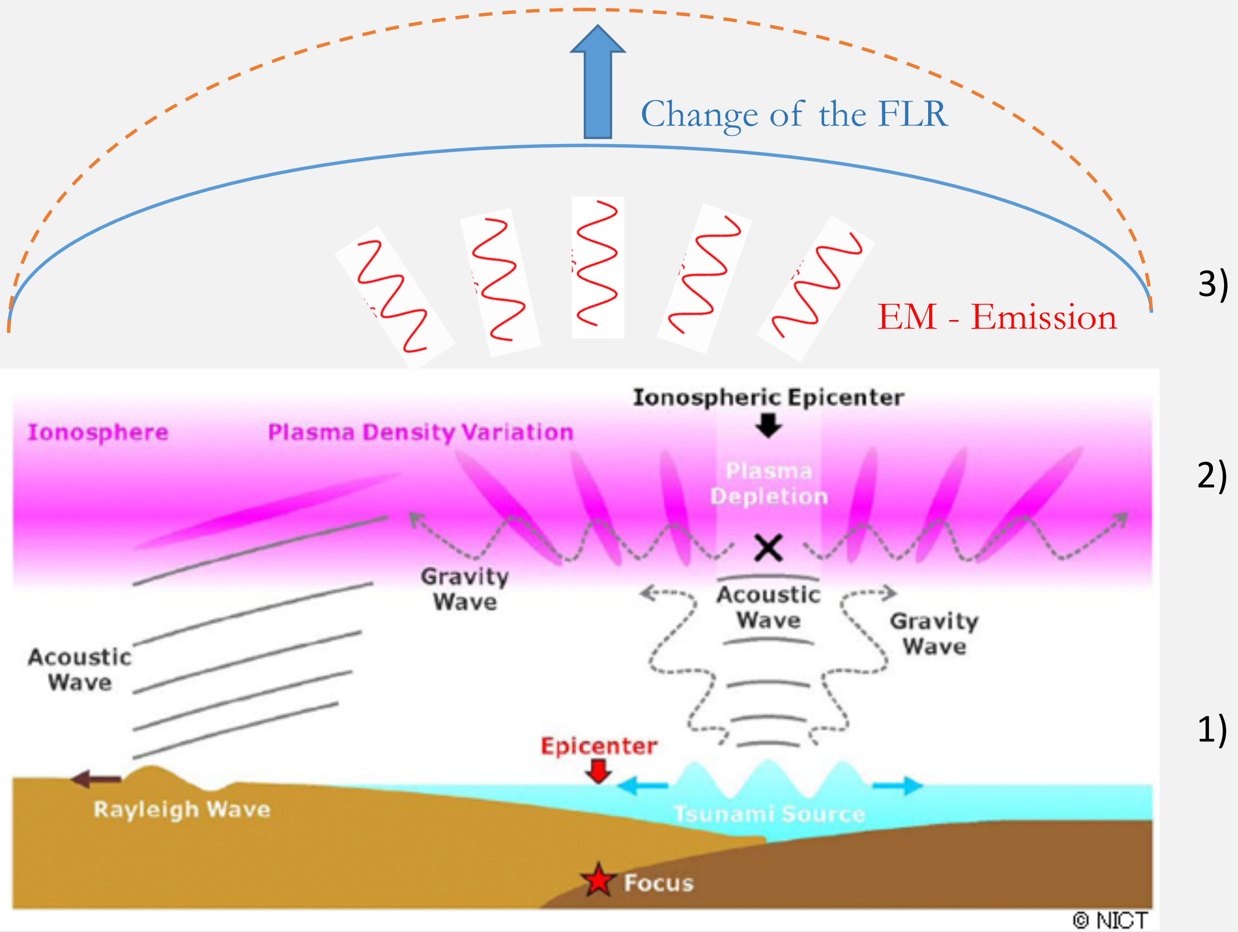

The model is based on three steps:

1) The earthquake generates an AGW, propagating through the atmosphere;
2) The AGW interacts with the ionosphere generating local instability in the plasma distribution through a pressure gradient
3) The ionospheric plasma variation generates EM waves propagating through the magnetosphere that interact with the magnetospheric field
4) The interaction causes a FL eigen-frequency change.
5) Since the FL is stretched, its eigen-frequency has to lower.

The MILC model

1- Piersanti M., Materassi, M., Battiston, R., Carbone, V., Cicone, A., D'Angelo, G.

Magnetospheric–Ionospheric–Lithospheric Coupling Model. 1: Observations during the 5 August 2018 Bayan Earthquake,
Remote Sensing 12 (20), 3299 (2020)

2 - Carbone, V., Piersanti, M., Materassi, M. , Battiston, R. , Lepreti F., Ubertini, P. ,
A mathematical model of lithosphere–atmosphere coupling for seismic events,
Sci Rep **11,** 8682 (2021)

3- Piersanti,M., Burger, W.J., Carbone, V., Battiston,R., Iuppa, R. and Ubertini, P.
On the Geomagnetic Field Line Resonance Eigenfrequency Variations during Seismic Event
Remote Sens. 2021, 13, 2839 (2021),

4 – In preparation: *A mathematical model of Atmospheric-Ionospheric coupling for seismic events*

Comprehensive analysis of an EQ

Example of Bayan Earthquake

Piersanti, Materassi, Battiston et al. 2020

The Bayan Earthquake CSES&other satellite/ground data

- On August 5, 2018 an earthquake stroked Indonesia.
- Mw= 6.8;
- λ=-8.3 °N - ϕ=116.5 °E;
- UT=11:46,34.

Orbit CSES #2797: 2018/08/05 - 05:20 - - 06:00 UT

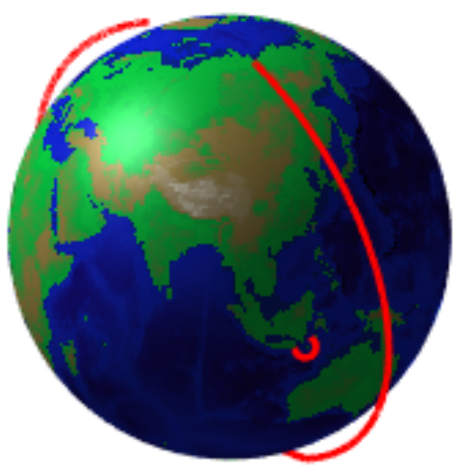

Terremoto di magnitudo **Mwp 6.8** del 05-08-2018 ore 13:46:34 (Italia) in zona: **Indonesia [Land]**

Dati Evento | Sismicità e Pericolosità | Impatto | Localizzazioni e Magnitudo | Meccanismo focale | Download

Un terremoto di magnitudo **Mwp 6.8** è avvenuto nella zona: **Indonesia [Land]**, il

- 05-08-2018 11:46:34 (UTC) 7 mesi fa
- **05-08-2018 13:46:34 (UTC +02:00) ora italiana**
- 05-08-2018 19:46:34 (UTC +08:00) orario locale nella zona del terremoto (Asia/Makassar)

con coordinate geografiche (lat, lon) **-8.3**, **116.5** ad una profondità di **10 km**.

Il terremoto è stato localizzato da: **Sala Sismica INGV-Roma**.

Ricerca terremoti: Qualsiasi nel raggio di 30 km

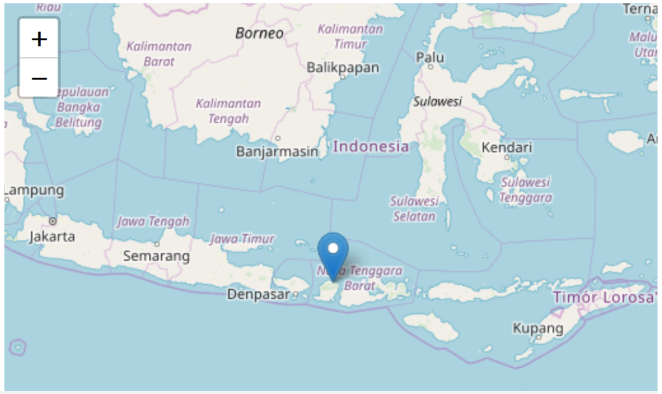

- CSES payloads: what did they observed?

August 5, 2018 – AGW observations

ERA-5 satellite data

Carbone, Piersanti, Materassi, Battiston et. al (2021)

Temperature Profile

- The potential energy density is defined as (VanZandt, 1985; Piersanti et al., 2020):

$$E_P = \frac{1}{2}\left(\frac{g}{N}\right)^2 \overline{\left(\frac{T'}{\overline{T}}\right)^2}$$

Where g is the gravitational acceleration (constant), N is the Brunt-Vaisala frequency defined as:

$$N = \sqrt{\frac{g}{\theta}\frac{d\theta}{dz}}$$

where $\theta = T\left(\frac{P_o}{P}\right)^{\frac{R}{c_p}}$ is the potential temperature, z is the altitude, P_0 is the standard reference pressure (1 hPa), R is the gas constant of air and c_p is the specific heat capacity at a constant pressure. R/c_p = 0.286 for air (Piersanti et al., 2020).

T' is the perturbation deviated from the background temperature $\overline{T}$ that are all function of the altitude. The variance term $\overline{\left(T'/_{\overline{T}}\right)^2}$ is calculated within a layer of 2 km thikness as:

$$\overline{\left(\frac{T'}{\overline{T}}\right)^2} = \frac{1}{z^{max} - z^{min}} \int_{z^{min}}^{z^{max}} \left(\frac{T'}{\overline{T}}\right)^2 dz$$

AGW evaluation – results

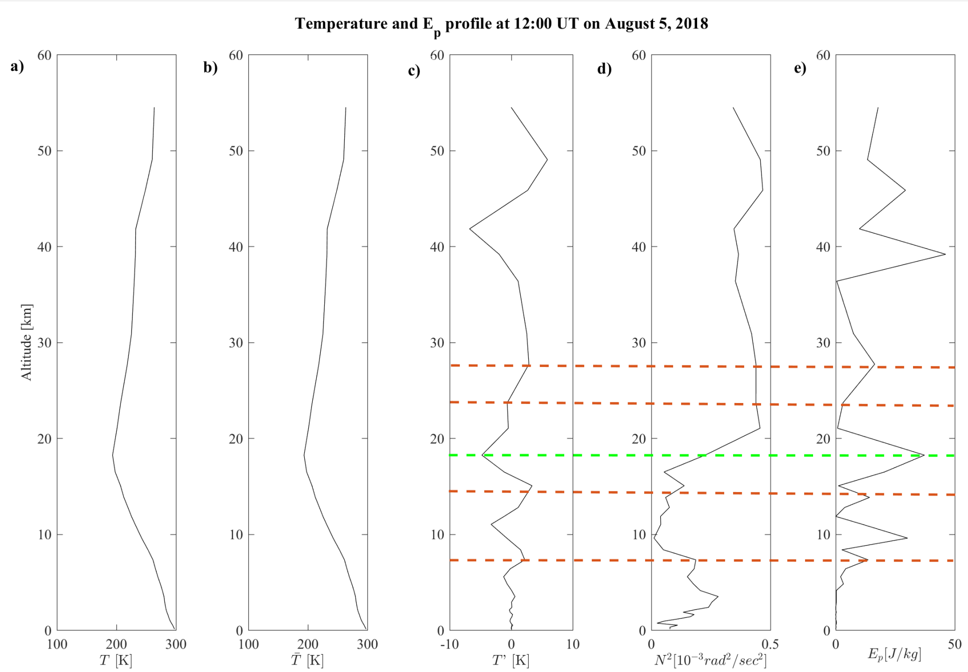

- The vertical wavelength of stratospheric AGW is about 2–10 km (Tsuda et al., 1994).
- The vertical temperature profile (left) at the EQ epicenter retrieved from ERA5 is hence filtered by a moving average (2 km), to obtain the background temperature profile (second panel from left);
- Then the temperature deviation (third panel) is computed by subtracting the background from the original temperature profile.
- Besides, the squared term of the Brunt-Väisälä frequency (Figure forth panel) can also be derived from the temperature profile. Finally, all the variables are substituted into equation (1),
- and the potential energy is calculated (right panel).
- The E_P value is absolutely maximum around the altitude of 17 km (the tropopause). The temperature inversion around this altitude is filtered out by the moving average. The similar increase can also be found in Brunt-Vaisala frequency.

- **Gravity waves disturb the temperature profile, and their influence is revealed in the temperature deviation profile (third panel).**
- **The wavelength is thus defined by a full period in the sinusoidal variation in the temperature deviation but not in the EP profile.**

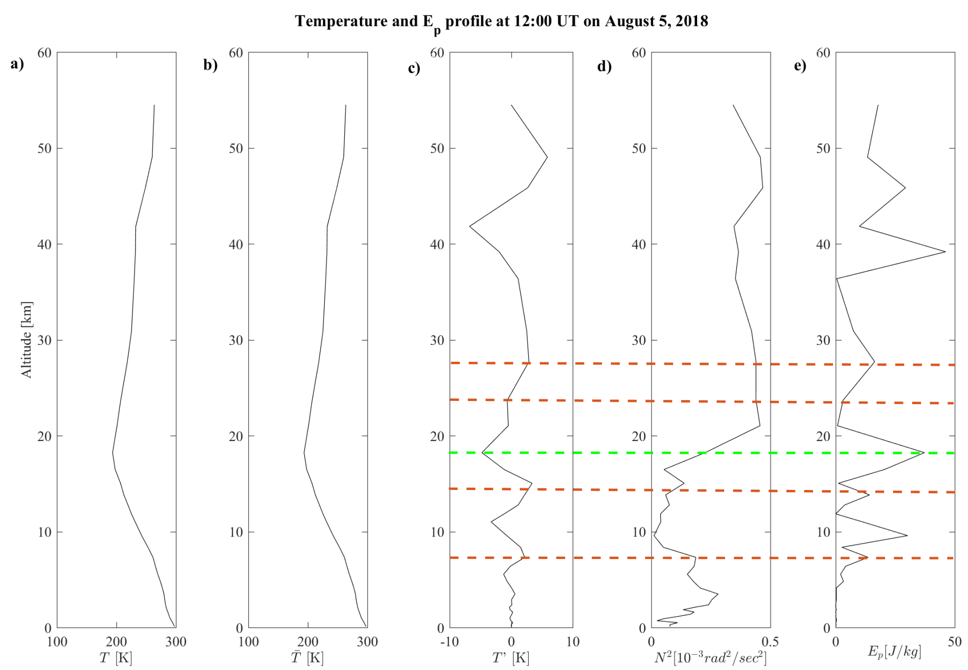

- Four wave crests are found in the temperature deviation profile at the altitudes of 17.8, 27.6, 36.6, and 44.8 km. There exist two sinusoidal periods, and the corresponding vertical wavelengths are 9.8 and 7.2 km, respectively.
- On the other hand, the *E*P profile maximizes only for the first wavelength.

So, there is a AGW of 9.8 km wavelength propagating in the atmosphere .

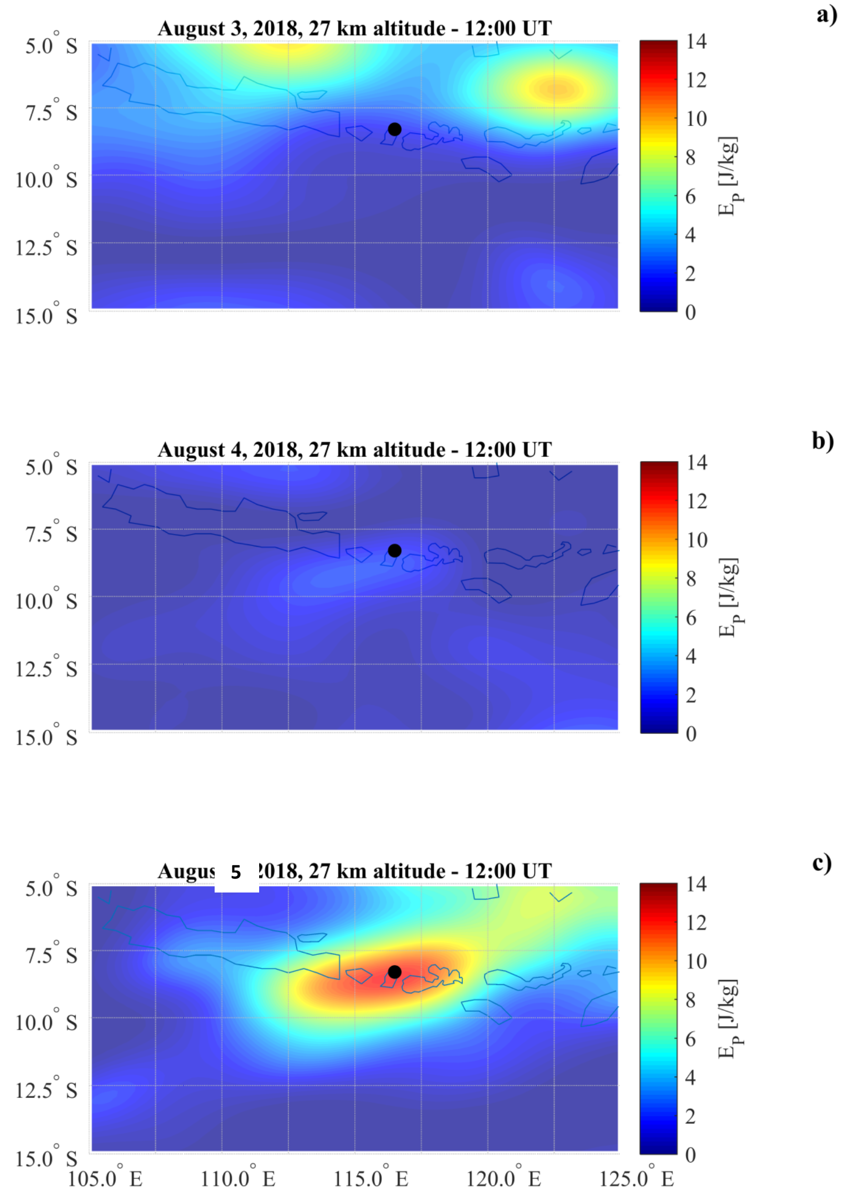

Temperature quiet

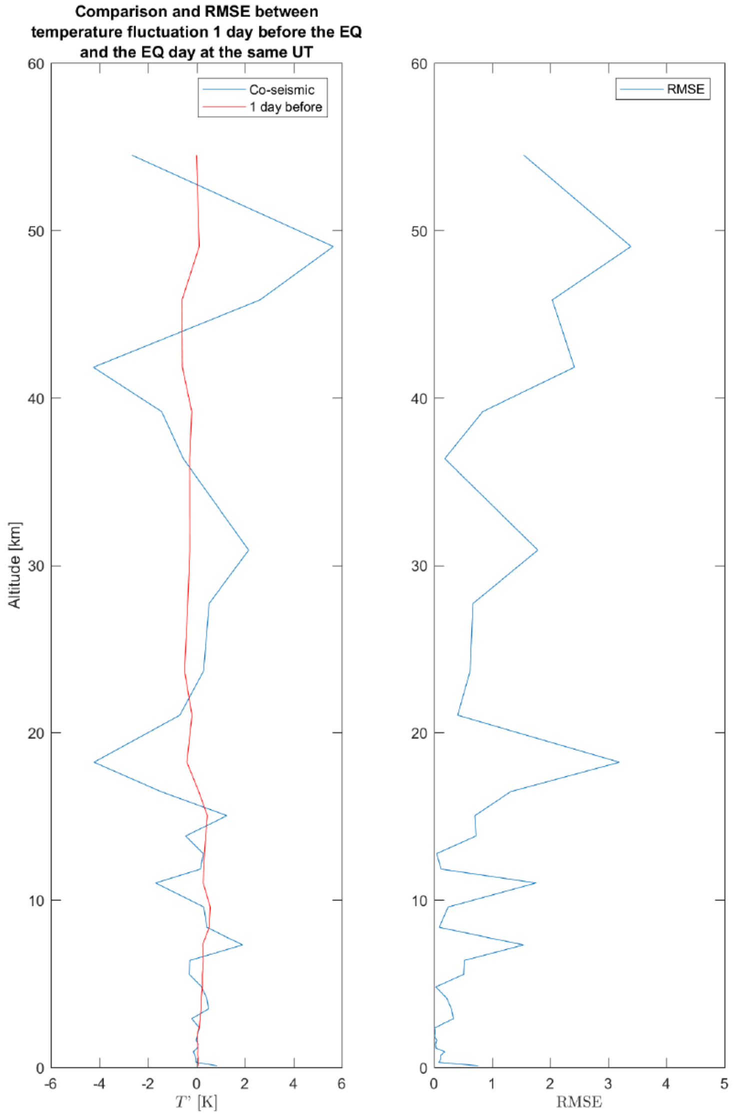

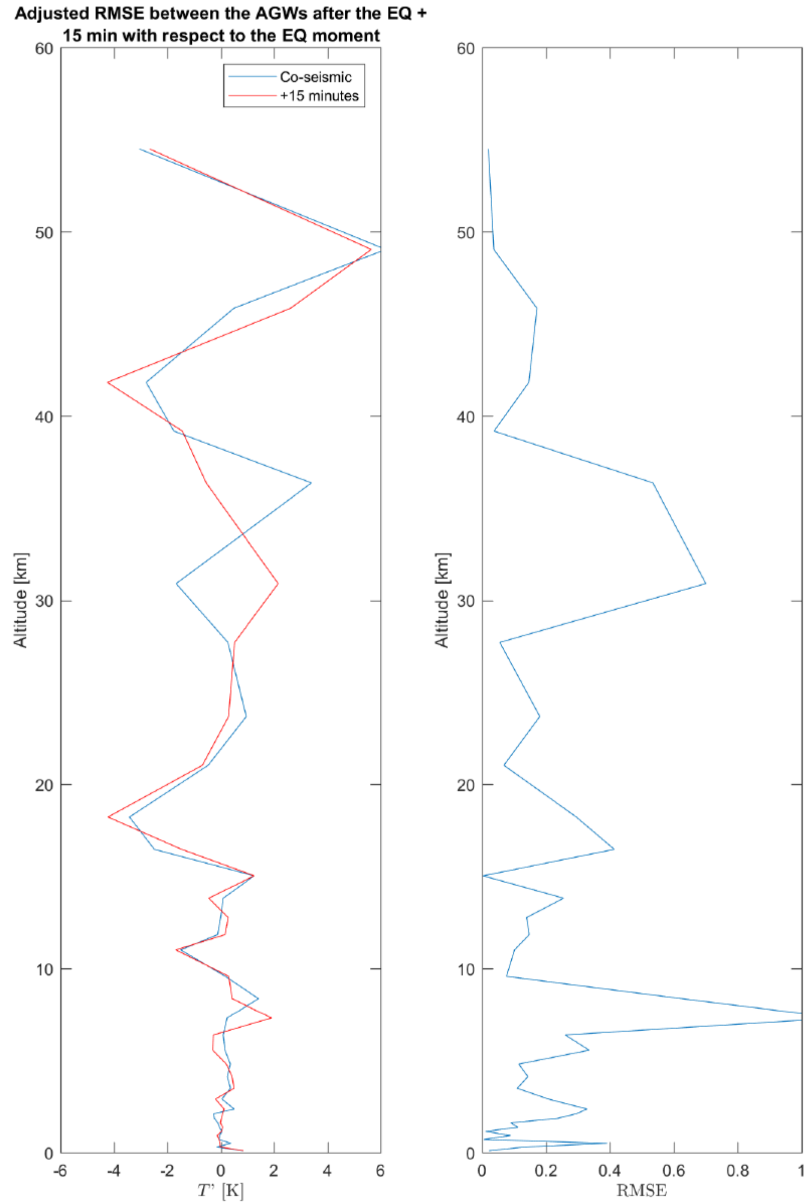

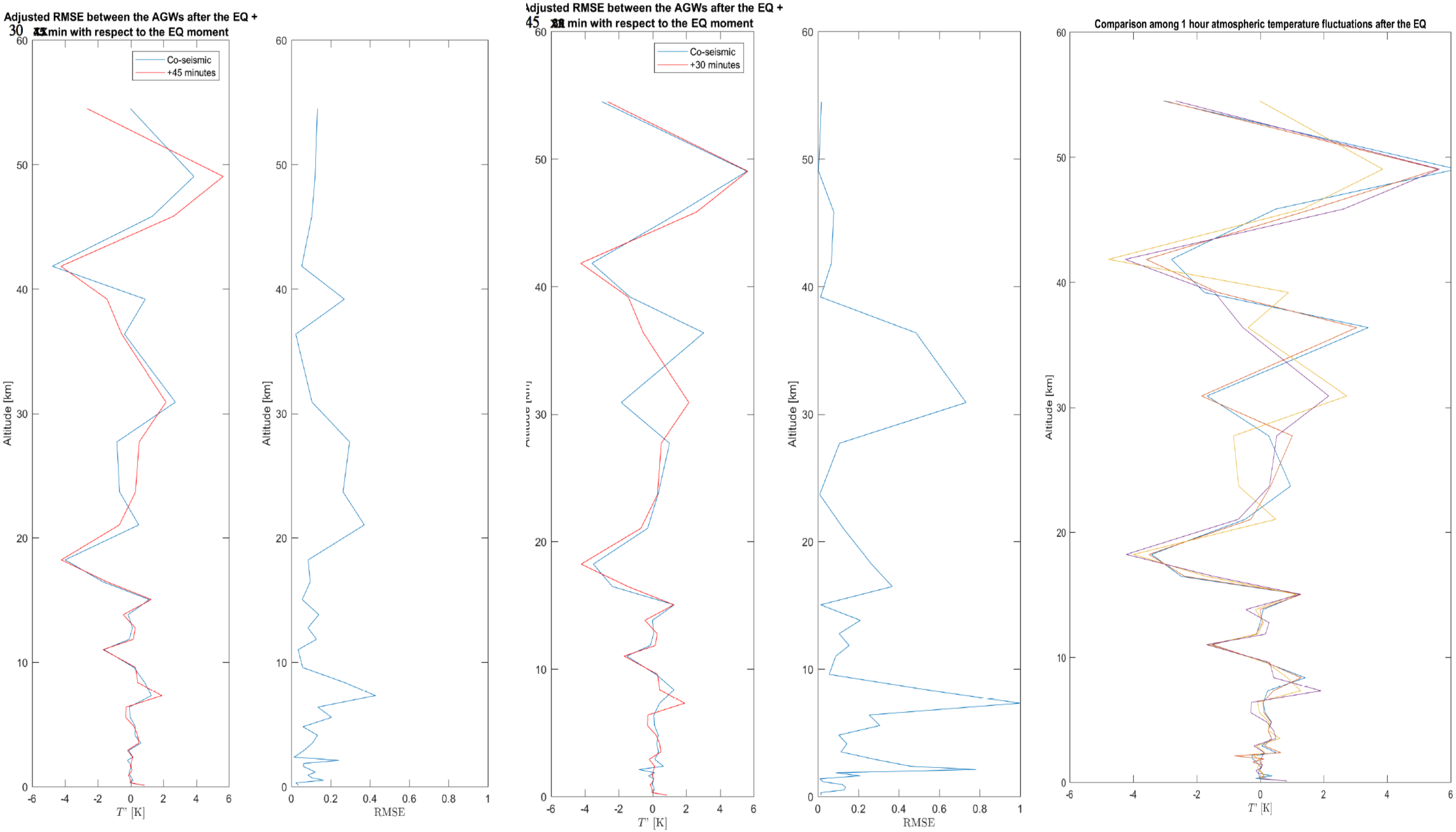
Adjusted RMSE between the AGWs after the EQ +
30 min with respect to the EQ moment
Co-seismic
+45 minutes
Altitude [km]
T' [K]
Altitude [km]
RMSE
Adjusted RMSE between the AGWs after the EQ +
45 min with respect to the EQ moment
Co-seismic
+30 minutes
T' [K]
Altitude [km]
RMSE
Comparison among 1 hour atmospheric temperature fluctuations after the EQ
Altitude [km]
T' [K]

August 5, 2018 – Ionospheric observations

TEC

Total Electron Content (TEC) from GPS

The observed modulation of the traveling time and direction of the signals (GHz) are sensitive to the electron density.

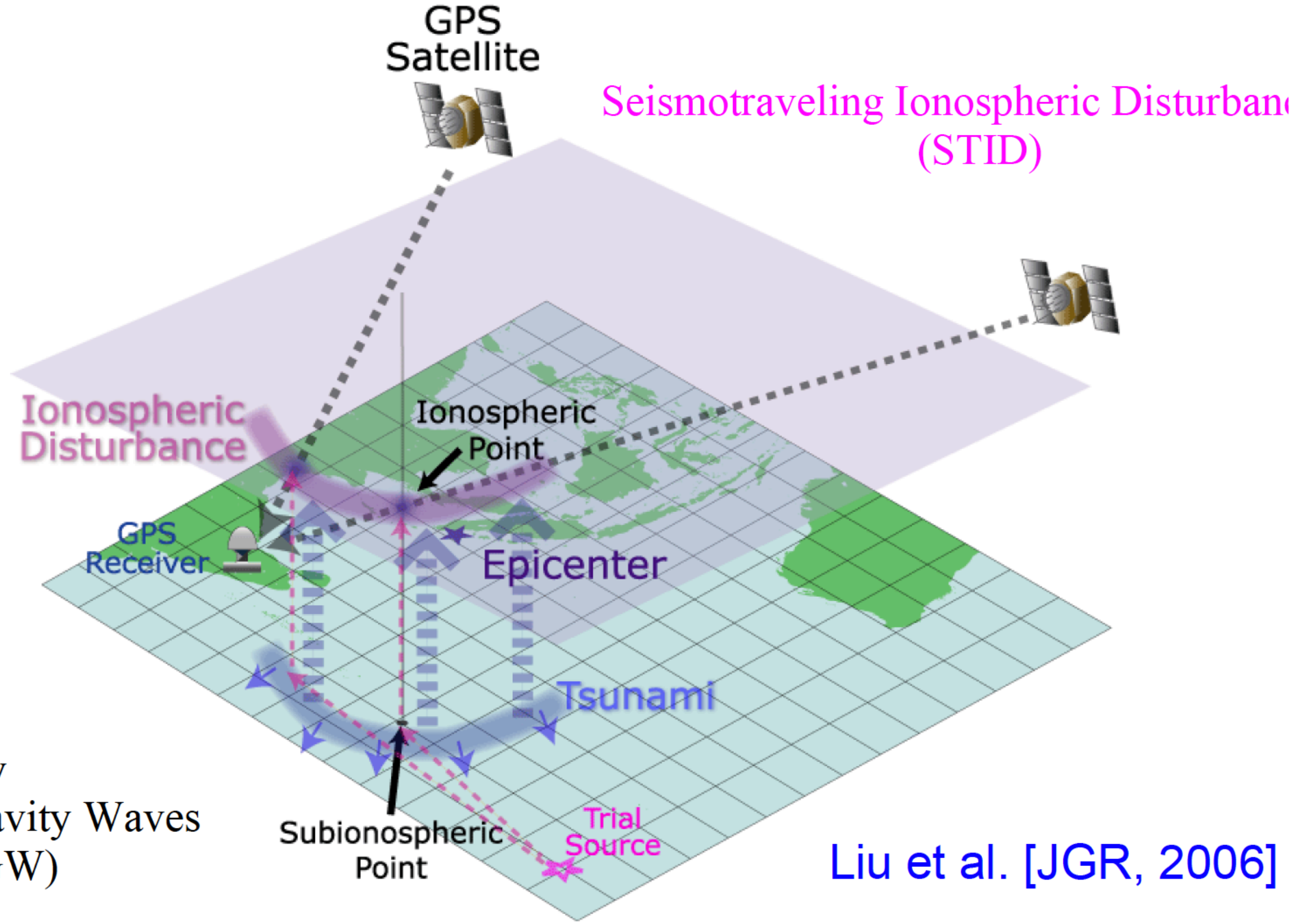

Generated by
Acoustic Gravity Waves
(AGW)

Liu et al. [JGR, 2006]

Total Electron Content (TEC)

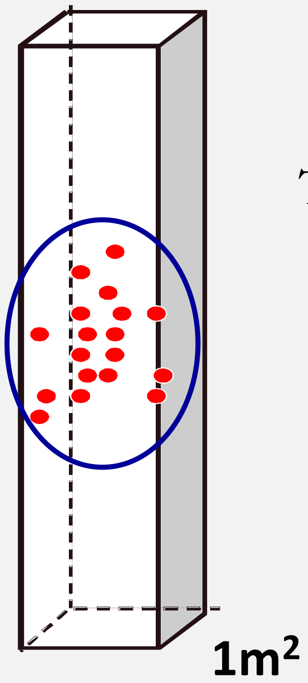

Total number of electrons in a column with cross section of 1m^2 along the satellite-receiver path (1 TECU = 10^{16} electrons/m^2)

$$TEC = \int_{h_{sat}}^{h_{rec}} N_e ds$$

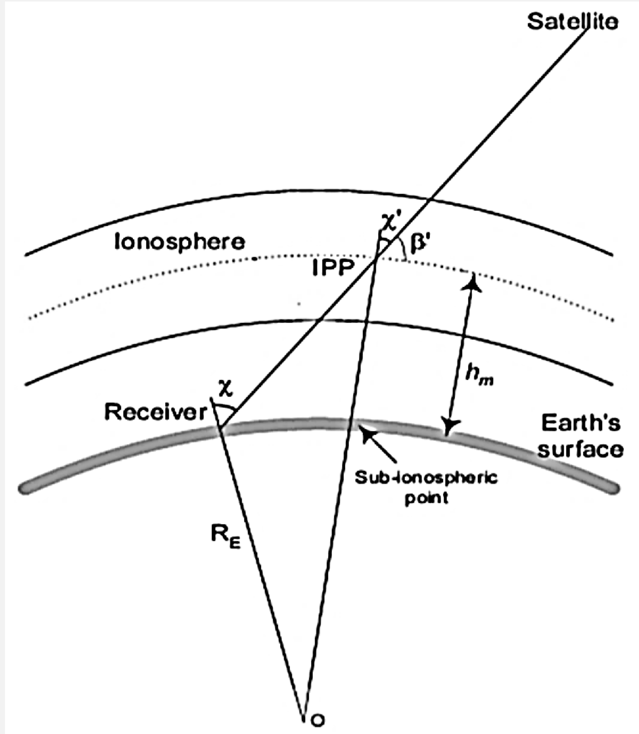

As TEC measurements take place at different elevation angles and are related to different ionospheric sectors, in order to obtain TEC values independent on the geometry of the GNSS constellation and on the receiver's network we verticalized TEC according to the following equation

$$vTEC = TEC\cos\left(\chi^{'}\right)$$

By assuming the ionosphere as a single thin ionized layer, located between 300 and 500 km above the Earth's surface, where the electron density maximizes

A glimpse on precursors.......

3- Bayan vTEC: August , 2018

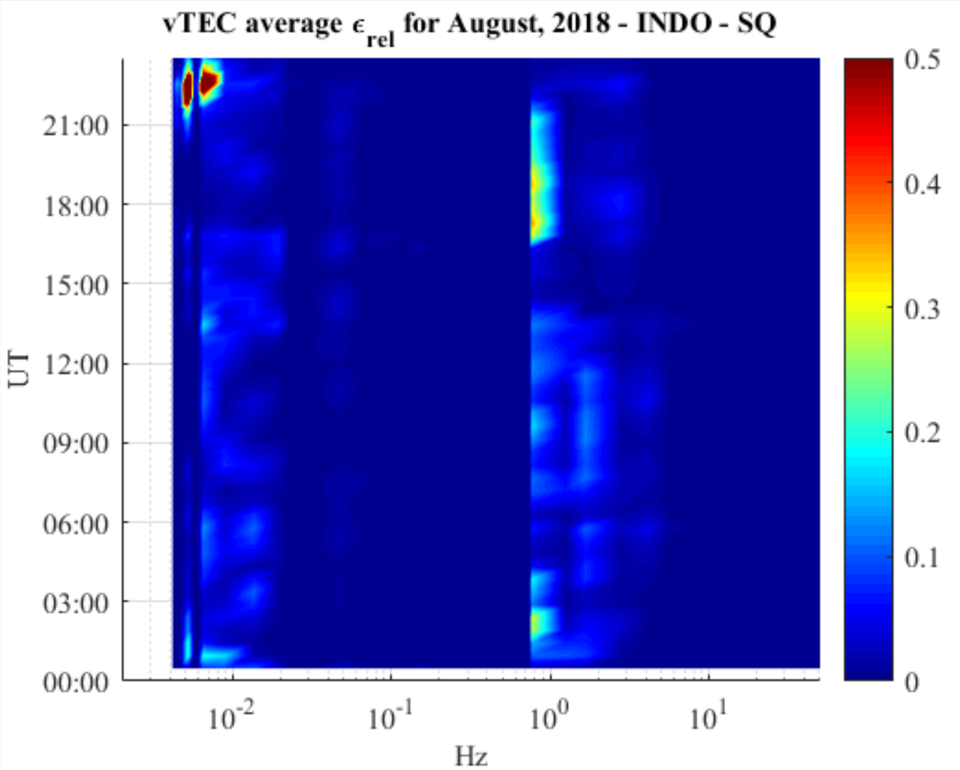

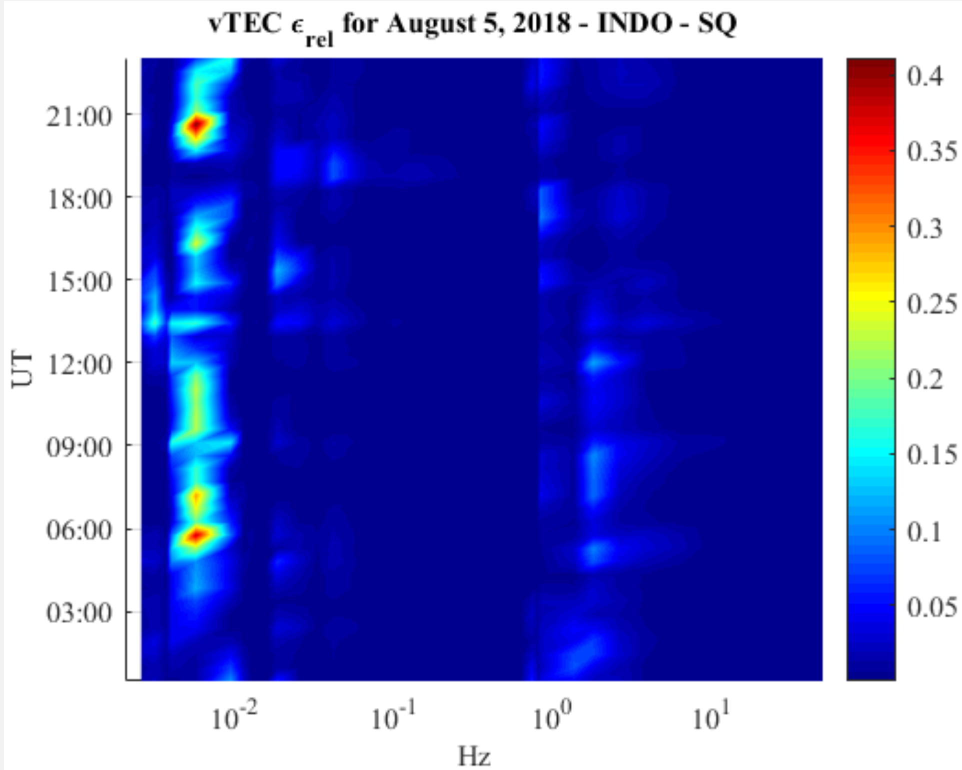

- Clear anomaly of vTEC with respect to monthly average.
- The first anomaly starts around 5:45 UT.
- The second anomaly starts around 09:00 UT with its peak at the EQ.
- Possible clear relation with EQ.

TID for case events - Maps

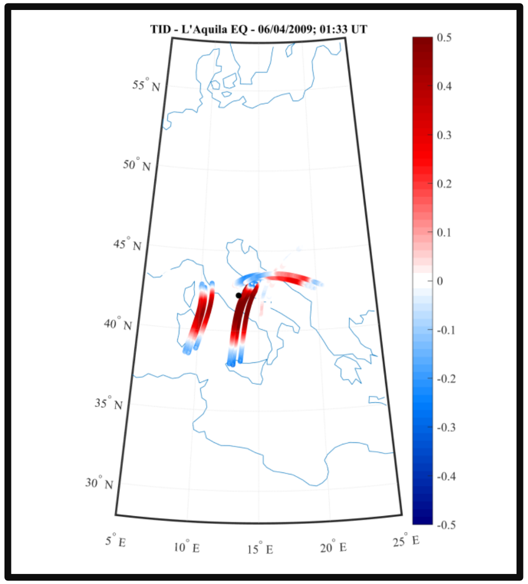

No TID as expected

TIDs as expected

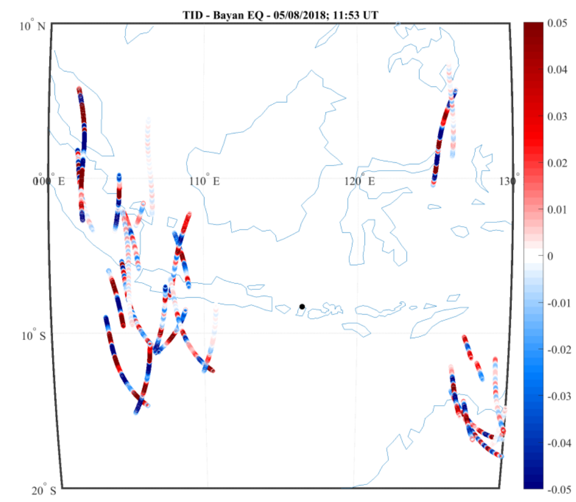

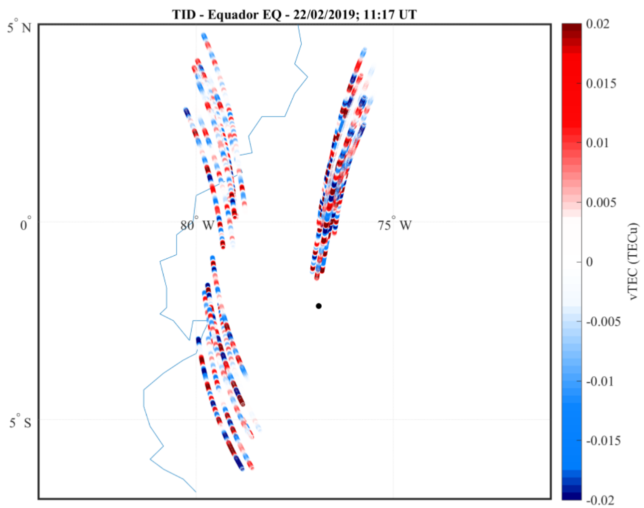

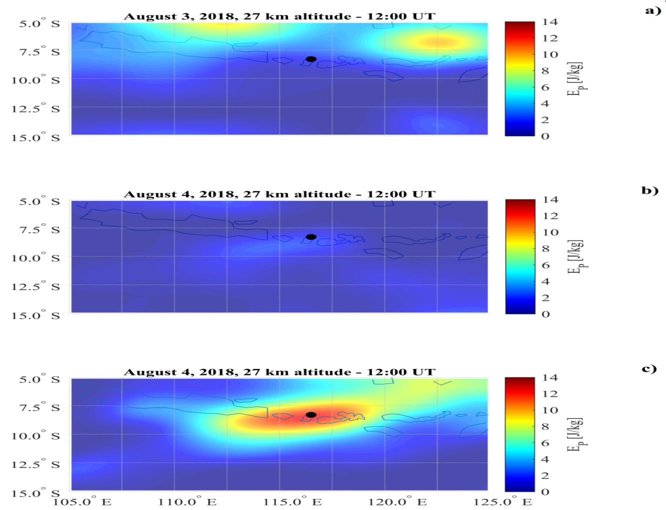

August 1-31, 2018 – ULF observations: Magnetic

- As for EFD we evaluated the Background

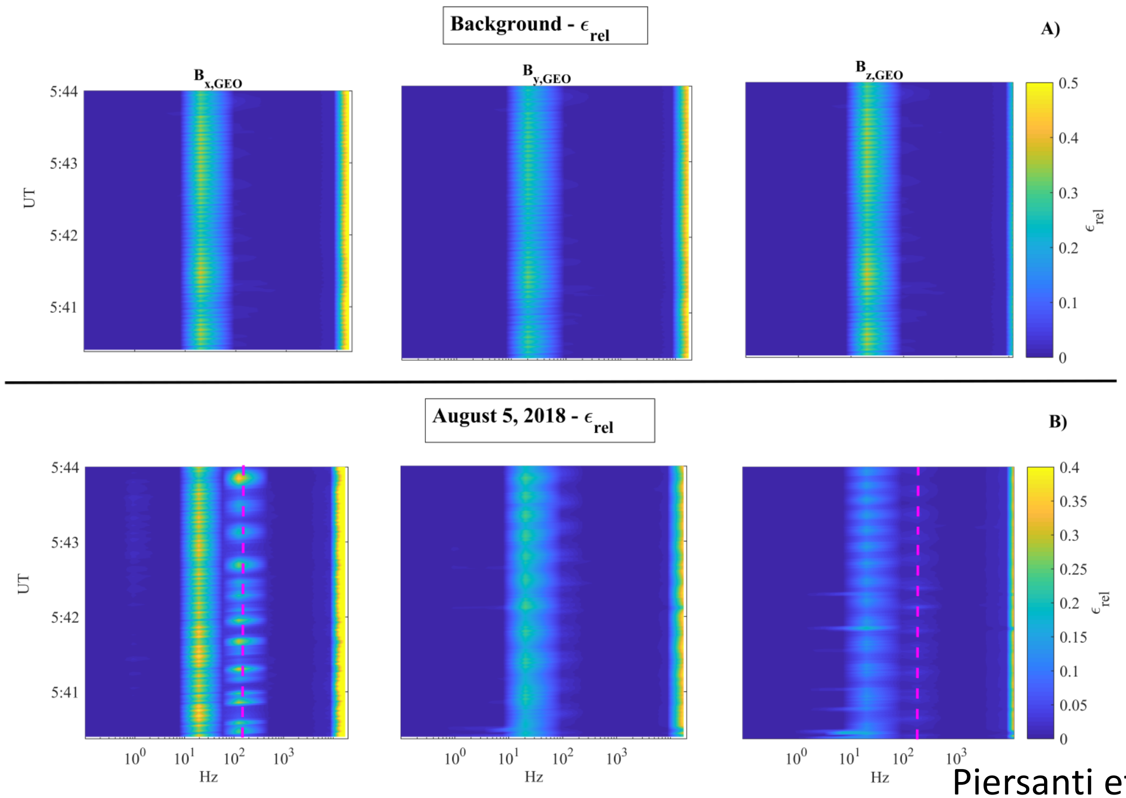

- A signature at ≈20 Hz is visible at all components, related to the Schumann ionospheric resonance at CSES orbit.
- The peak around 12 kHz is the signature of the lower-hybrid resonance of the ionosphere F2 layer.

Piersanti et al. *Remote Sens.* **2020**, *12*, 3299; doi:10.3390/rs12203299

- Anomalous peak (magenta line) at 180 Hz with respect to the background has been detected along the Bx and Bz component.
- **Interestingly, this oscillation is perpendicular to the one detected to the EFD. It is an EM wave!**

August 1-31, 2018 – ULF observations: Electric

- On the basis of Piersanti et al. [2020], we first evaluated both the environmental and the instrumental background over Bayan cell [3°x3° - latxlon] for SQ and M<2 conditions.

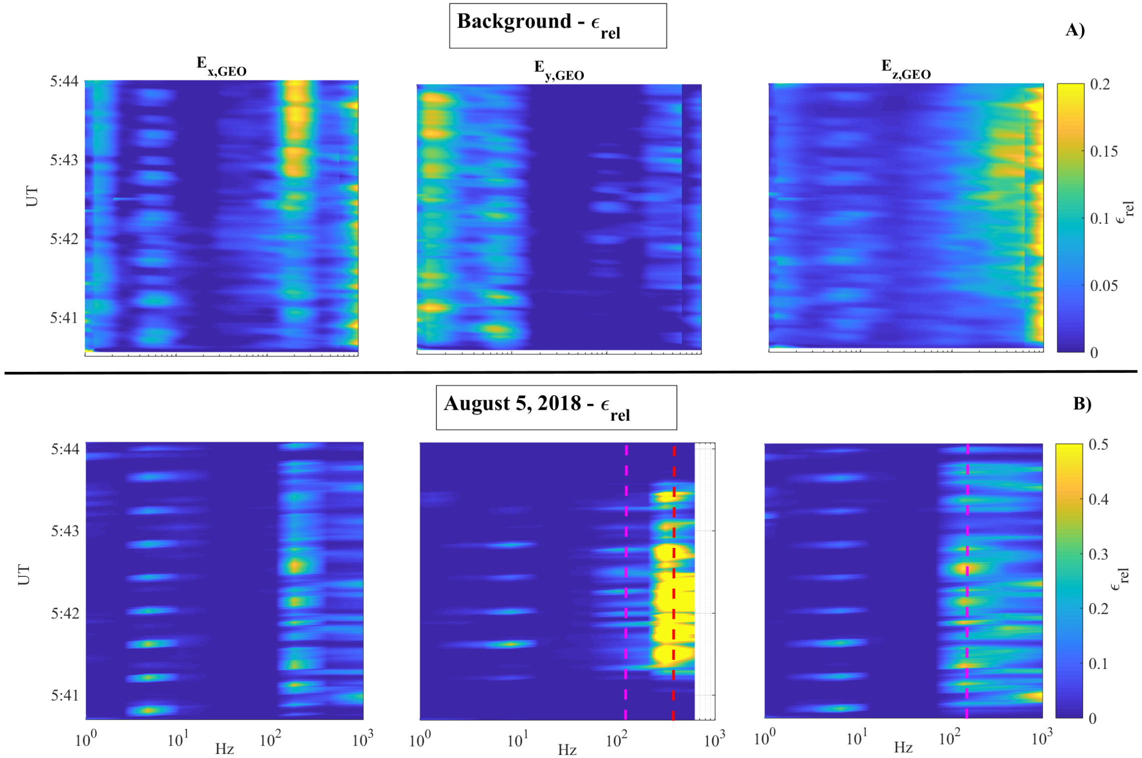

- A signature (pink circle) at ≈8 Hz is visible at all components, related to the Schumann ionospheric resonance at CSES orbit.
- The peaks detected at frequency around 2 Hz are due to the VxB electric field present in the ELF band.
- The peak around 1kHz is the signature of the Plasmaspheric hiss [Balazs, 2008; Vellante et al, 2014; Zhima et al., [2019].
- The peak around 250-300 Hz are a portion of the whistler mode chorus generated around L=5 propagating into the plasmasphere [Li et al. 2009; Zhima et al., 2019].

Piersanti et al. *Remote Sens.* **2020**, *12*, 3299; doi:10.3390/rs12203299

- Anomalous peaks at 180 Hz (E_y and E_z component, magenta) and at 630 Hz (E_y component, red line) with respect to the background has been detected.

August 5, 2018 – Poynting flux

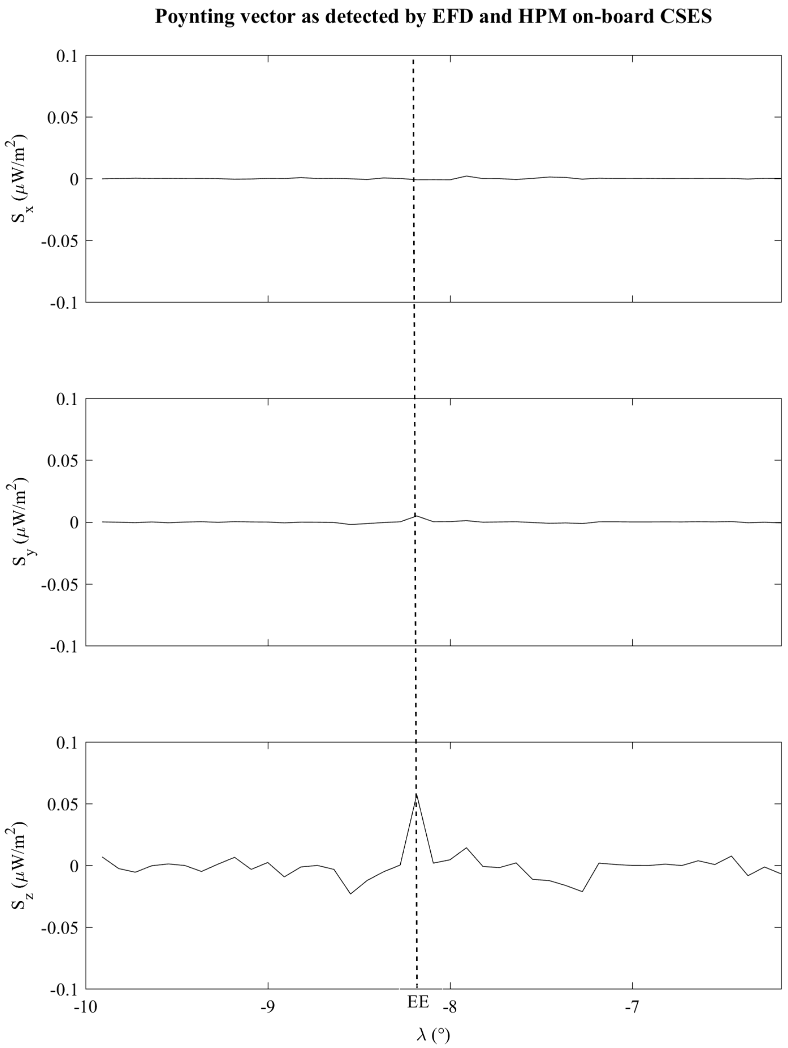

- The Poynting flux analysis confirms the injection of EM wave coming from downward.

Piersanti et al. *Remote Sens.* **2020**, *12*, 3299; doi:10.3390/rs12203299

August 5, 2018 – FLR frequency observations Ground Stations

FLR

Battiston,   Burger, Piersanti, Iuppa in preparation (2021)

On the Geomagnetic Field Line Resonance Eigenfrequency Variations during Seismic Event

Mirko Piersanti [1,*], William Jerome Burger [2,3], Vincenzo Carbone [4], Roberto Battiston [2,5], Roberto Iuppa [2,5] and Pietro Ubertini [1]

Remote Sens. **2021**, *13*, 2839. https://doi.org/10.3390/rs13142839

Gradient method for detecting field line resonances from ground-based ULF measurements

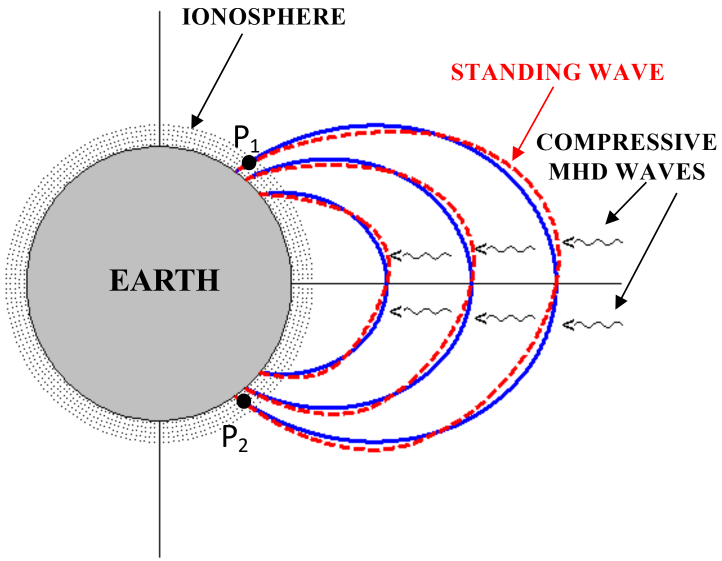

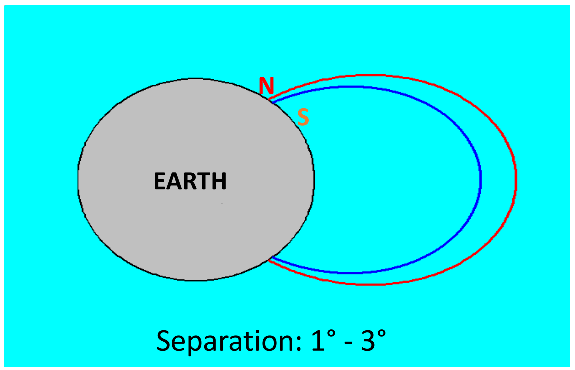

Higher latitude field line → Lower resonance frequency (f_N)

Lower latitude field line → Higher resonance frequency (f_S)

$$T(L) \cong \int_{P_1}^{P_2} \frac{ds}{V_A(s)}$$

V_A: Alfvén velocity

$$T(L) = 2\mu_o \int_{P_1}^{P_2} \frac{\rho^{1/2}(s)}{B(s)} ds$$

FREQUENCY RESPONSE OF TWO OSCILLATORS

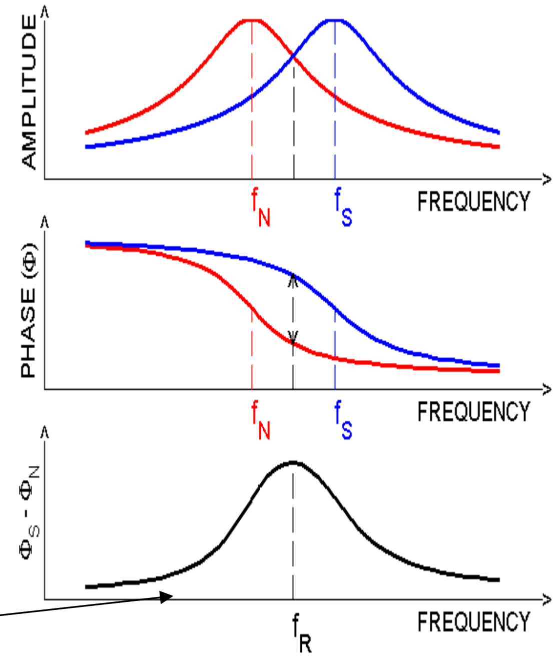

CROSS-PHASE TECHNIQUE

Resonance frequency at the middle point.
Identified by a maximum in the phase difference

FLR	Date	UTC Time	Kp	M	Latitude	Longitude	Region
X	17/07/2001	14.50.57	0	6.3	3.061° S	148.180° E	Bismarck Sea
X	27/11/2002	00.17.20	1	5.4	12.279° N	120.753° E	Philippines
X	12/12/2003	08.07.30	1	5.2	0.110° S	123.991° E	Indonesia
X	28/01/2004	07.41.04	1	5.7	4.931° S	153.584° E	New Guinea
-	09/02/2006	05.44.30	2	6.2	4.810° S	133.063° E	Indonesia
X	17/05/2006	01.21.26	1	6.0	3.743° S	144.305° E	New Guinea
X	24/06/2006	00.03.07	1	6.3	3.071° S	127.183° E	Indonesia
X	16/09/2007	01.20.38	2	6.4	2.763° S	101.106° E	Indonesia
-	26/10/2007	16.34.47	0	6.0	3.271° S	143.763° E	New Guinea
X	14/11/2007	17.44.04	2	5.7	23.215° S	70.526° W	Chile
-	25/07/2008	20.11.07	1	6.5	5.808° S	146.658° E	New Guinea
X	11/09/2008	00.00.02	1	6.6	1.885° N	127.363° E	Indonesia
-	19/12/2008	00.34.58	2	6.8	20.372° N	146.339° E	Mariana Islands
X	06/01/2009	19.56.25	2	6.0	0.566° S	132.784° E	Indonesia
X	16/02/2009	00.33.36	2	6.1	3.664° S	149.608° E	Bismarck Sea
X	02/03/2009	00.03.39	1	6.5	1.105° S	119.868° E	Indonesia
X	25/07/2009	18.41.58	2	5.8	1.869° N	97.020° E	Indonesia
X	15/10/2009	03.34.28	1	6.0	1.111° N	85.322° W	Ecuador
-	24/02/2008	04.36.29	2	6.5	3.741° S	101.986° E	Indonesia
NA	07/06/2008	19.10.48	2	5.0	3.552° S	140.851° E	Indonesia
-	02/07/2008	00.08.31	2	5.2	12.451° N	44.202° W	Mid-Atlantic
X	07/02/2008	23.16.41	1	5.3	17.558° N	144.922° E	Mariana Islands
-	19/12/2006	12.48.16	2	6.0	2.458° N	98.000° E	Idonesia
X	16/11/2009	18.34.24	0	5.2	19.556° S	70.365° W	Chile
NA	11/01/2009	14.03.49	1	5.6	6.388° S	147.423° E	New Guinea
NA	11/01/2009	14.15.54	1	5.0	0.769° S	133.506° E	Indonesia
X	16/09/2008	21.47.14	2	5.7	17.438° N	73.915° E	India
X	24/05/2003	01.46.06	1	5.9	14.428° N	53.813° E	Owen region
-	14/11/2007	18.55.49	2	5.1	22.670° S	70.292° W	Chile
NA	26/10/2007	16.34.47	1	5.6	3.271° S	143.7630 E	New Guinea
X	22/11/2003	09.30.03	1	5.1	13.281° N	57.466° E	Arabic Sea
X	12/03/2008	01.32.34	2	6.0	1.934° N	132.519° E	Indonesia
X	02/02/2013	14.17.33	1	6.9	42.8° N	143.27° E	Japan
-	25/10/2013	17.10.16	2	7.1	37.194° N	144.66° E	Japan
X	06/10/2017	07.59.32	1	6.2	37.325° N	144.02° E	Japan
X	08/01/2019	12.39.31	2	6.3	30.526° N	131.113° E	Japan
X	18/06/2019	13.22.22	0	6.4	38.563° N	139.504° E	Japan
X	27/07/2019	18.31.07	1	6.3	33.015° N	137.413° E	Japan
X	19/04/2020	20.39.08	2	6.3	38.858° N	141.99° E	Japan
-	21/11/2016	20.58.47	1	6.9	38.296° N	141.642° E	Japan
X	05/08/2018	11.58.00	0	6.5	8.28° S	116.4° E	Indonesia
X	25/04/2015	06.45.21	2	6.6	28.18° N	84.72° E	Nepal

Statistical analysis for the Ionosphere-Magnetosphere coupling during EQ

- We made a statistical analysis of the possible FLR signature associated to EQ in the time span from 2001-07-17 and 2020-08-31.

- We selected 42 case events for which the planetary geomagnetic Kp index [Matzka et al., 2021] is lower than 3 in order to exclude any possible variation of solar origin;

- To evaluate the *f**, we studied the cross-space spectrum [Waters et al., 1994] between the North-South magnetic field components observed at two geomagnetic observatories close enough to the EQ epicentre location

Statistical analysis for the Ionosphere-Magnetosphere coupling during EQ

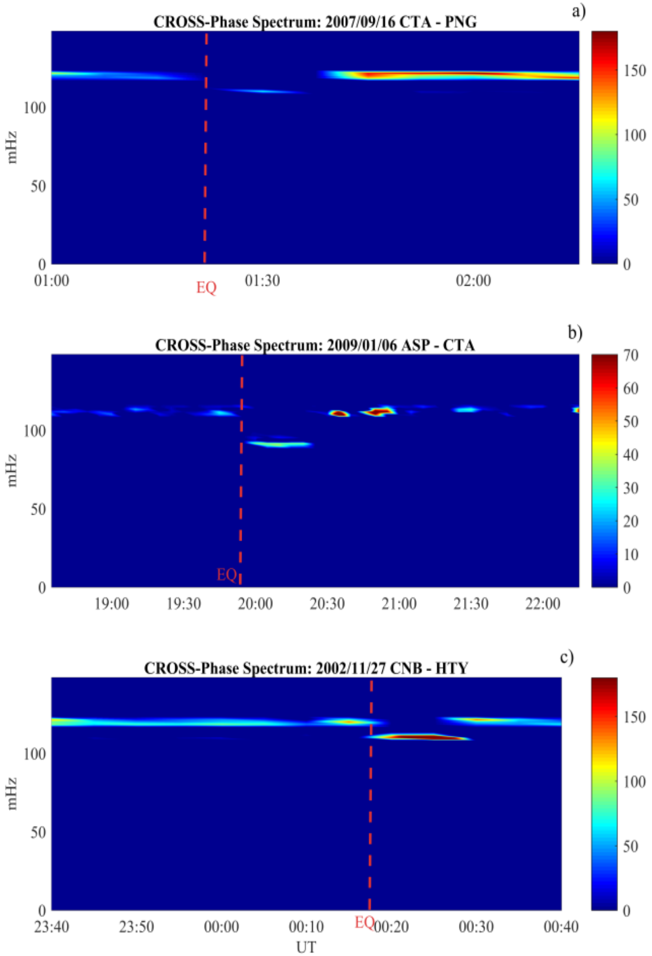

- We found 28 cases out of 42 in which there is a clear variation of the estimated f^* (indicated with the "X").
- In 4 cases it was not possible to correctly evaluate f^* because of the post-sunset occurrence of the EQ (indicated with the "NA").
- Finally, no f^* variations has been detected for 10 case events (indicated with "-").

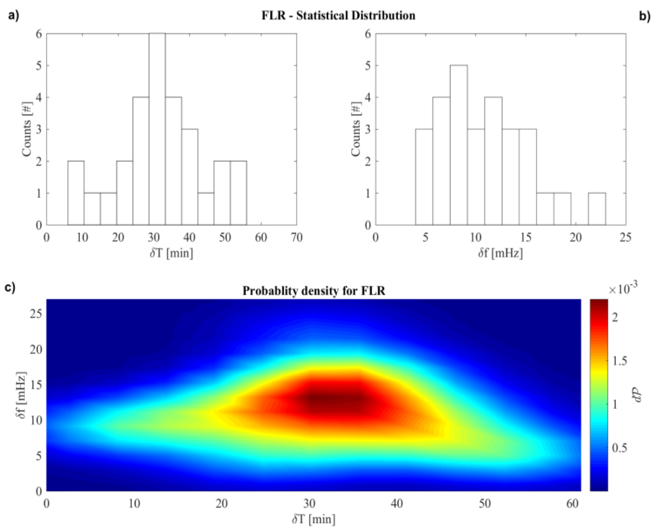

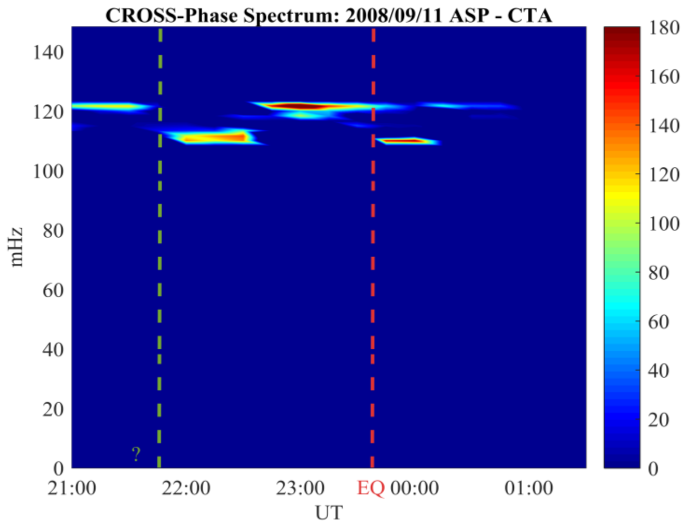

- The co-seismic FLR eigenfrequency variation is characterized by a frequency decrease of 12±3 mHz and a time duration of 36±3 min.

August 5, 2018
Van Allen Belt electron bursts linked to EQ

PEB

Battiston et al. in preparation (2022)

Trapped Particle Motion in the Van Allen Radiation Belts

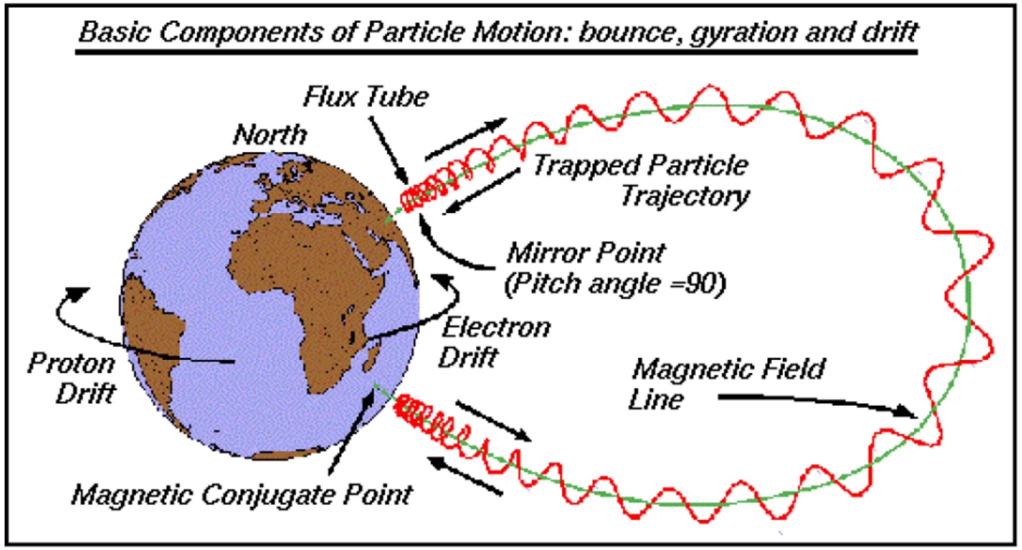

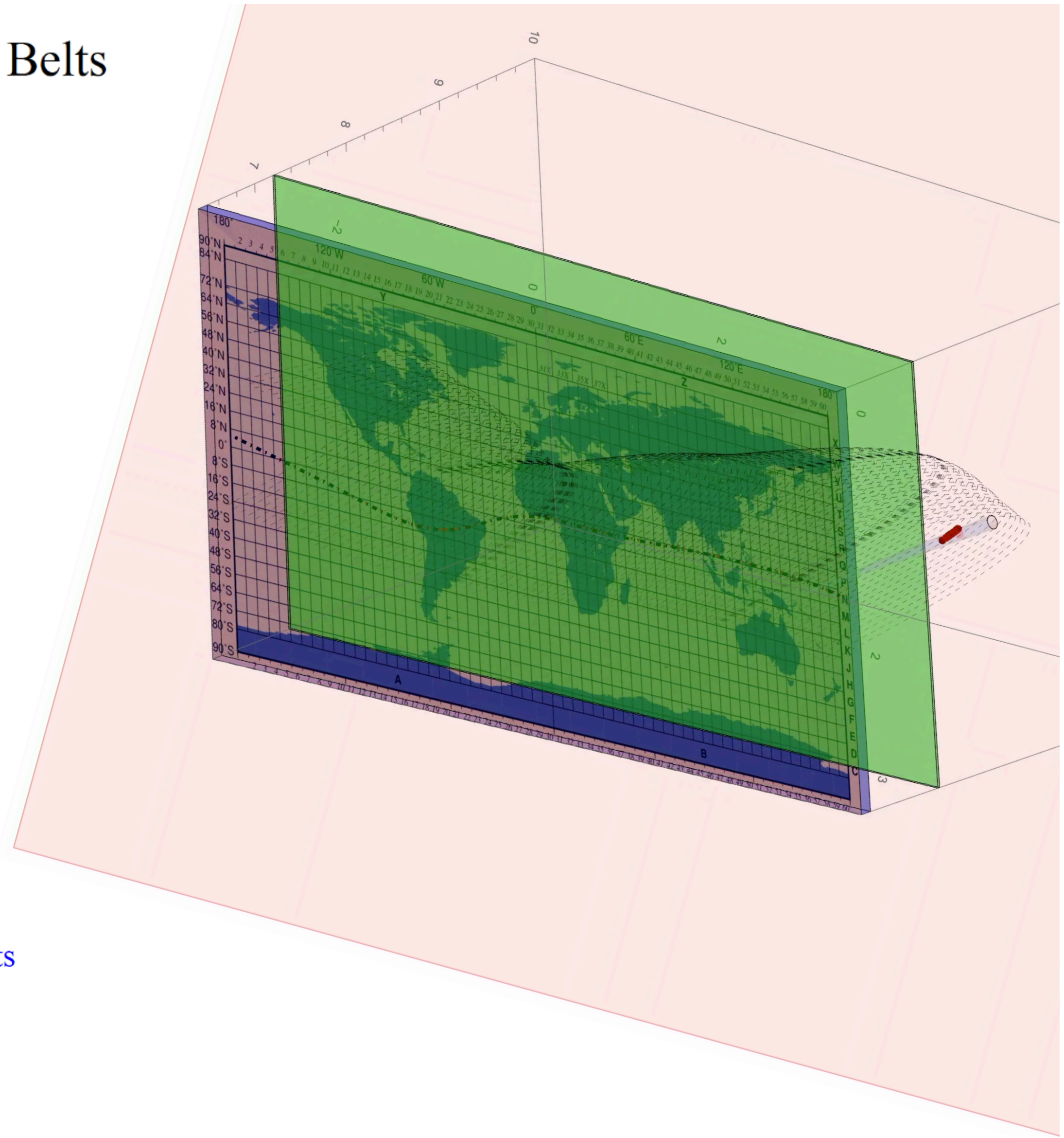

$$J_1 = \frac{\pi p_\perp^2}{qB} \qquad \frac{p^2 \sin^2 90^o}{2m_o B_m} \overset{I}{=} \frac{p^2 \sin^2 \alpha}{2m_o B}$$

Gyration orbit (pitch angle)
constant magnetic moment

$$\frac{J_2}{2p} = \frac{1}{2}\oint \cos\alpha \, ds = \int_{s_m}^{s'_m} \sqrt{1 - \frac{B(s)}{B_m}} \, ds$$

Bounce motion between mirror points
integral invariant

$$J_3 = q \oint \boldsymbol{B} \cdot \boldsymbol{dS} = q\Phi = q \int_{R_o}^{\infty} B_o \left(\frac{R_E}{r}\right)^3 2\pi r dr$$

Longitudinal Drift
flux invariant

Nat. Hazards Earth Syst. Sci., 8, 1277–1291, 2008

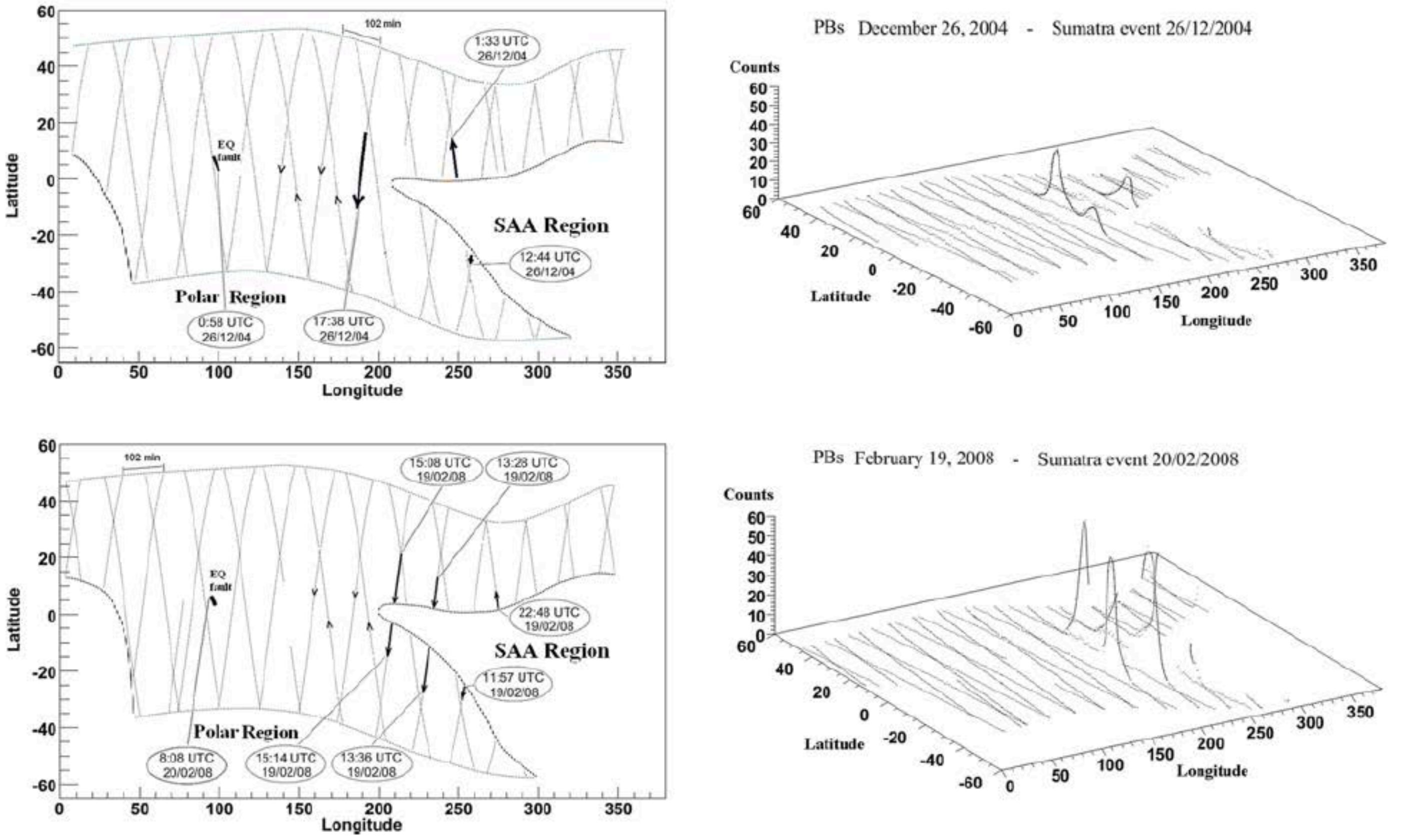

Fig. 7. The NOAA-15 orbits, PBs geographical distribution, PB times with respect to the Sumatra EQ times and fault positions (on the left), and the NOAA-15 PB count dynamic (on the right) are shown in two cases. In the first case we can only observe post-seismic PBs while in the second we can observe pre-seismic PBs. Bold lines define the selection of particle precipitation outside the SAA while the dotted lines indicate the polar regions with L>2.2 and arrows define the direction of the satellite motion.

Drift Time and Equatorial Pitch Angle: Approx. Loss Cones Classification

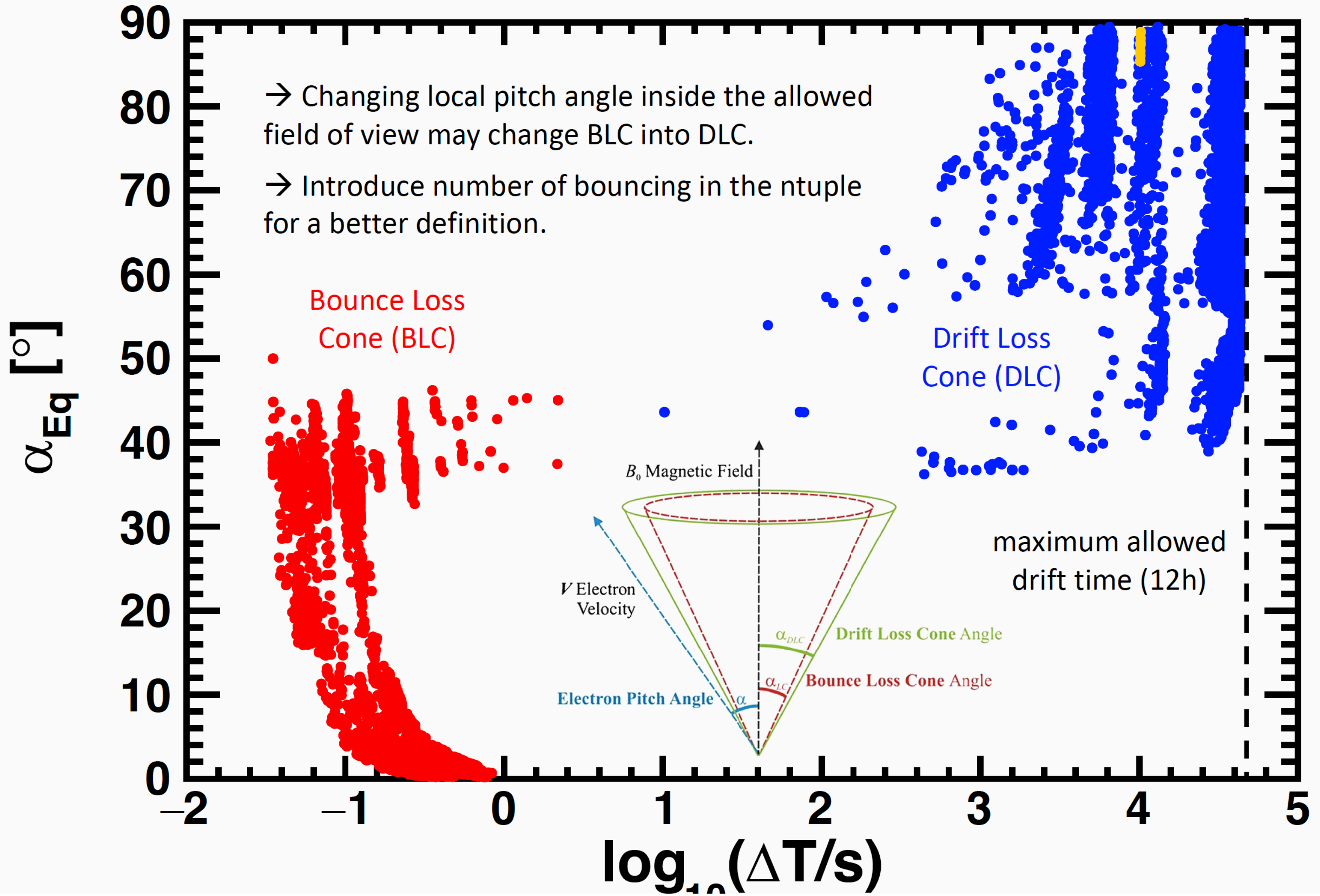

Minimum Distance to the Earthquake Vertical

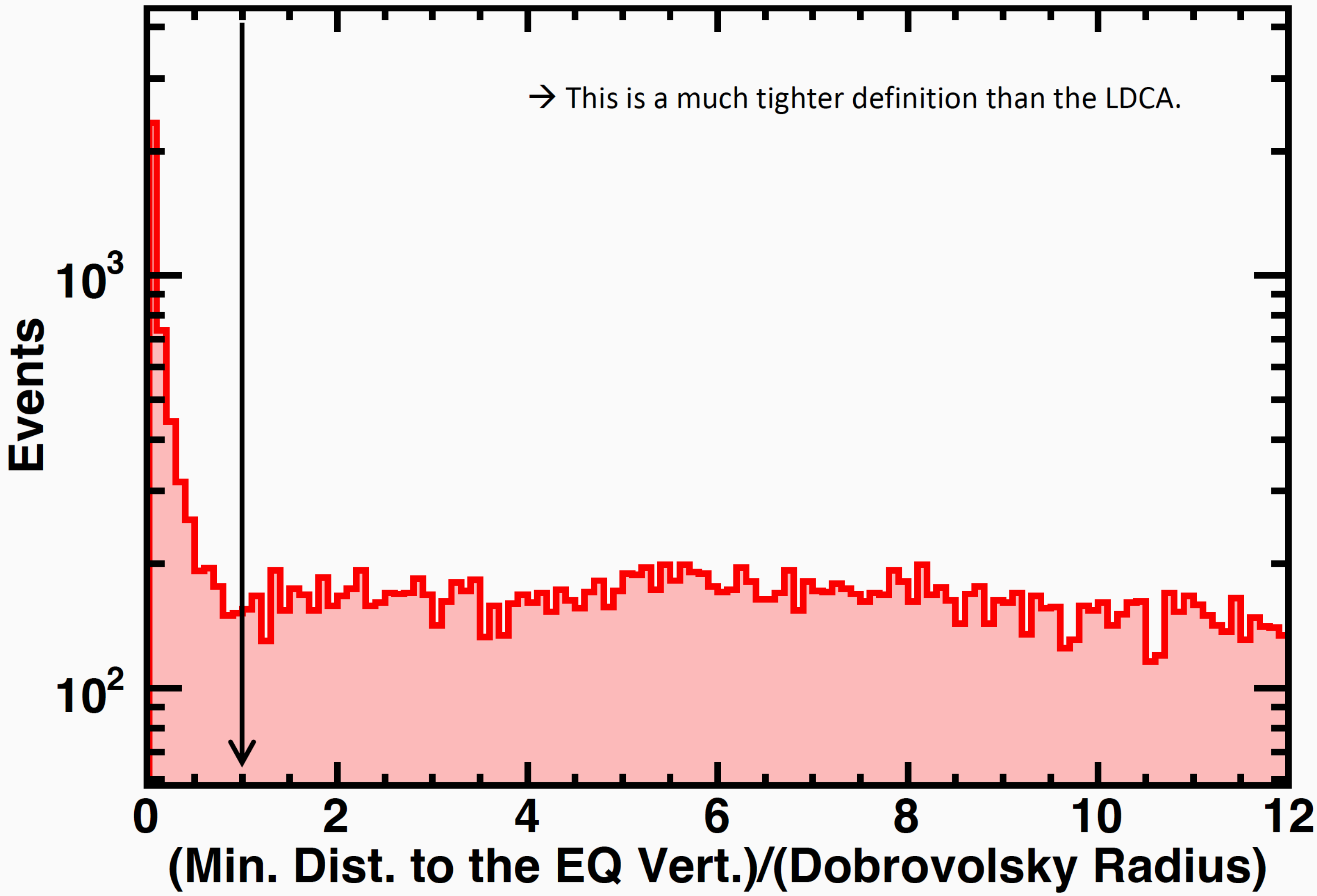

Conclusions

- Coupling between litosphere and magnetosphere has been demonstrated for EQ of magnitude M > 5 Richter Scale
- Local and global non imaging observables from space and from ground define a clear causal sequence of couling events linking ground to space
- The MILC model provides for the first time quantitative predictions which can be verified experimentally with great accuracy
- Use of this technique for tsunami forecasts seem possible and will be investigated
- Using the causal coupling approach based on the measurements of AIMI invariants study of EQ precursor phenomena can be studied based on solid physical evidence and methods


That's all Folks!

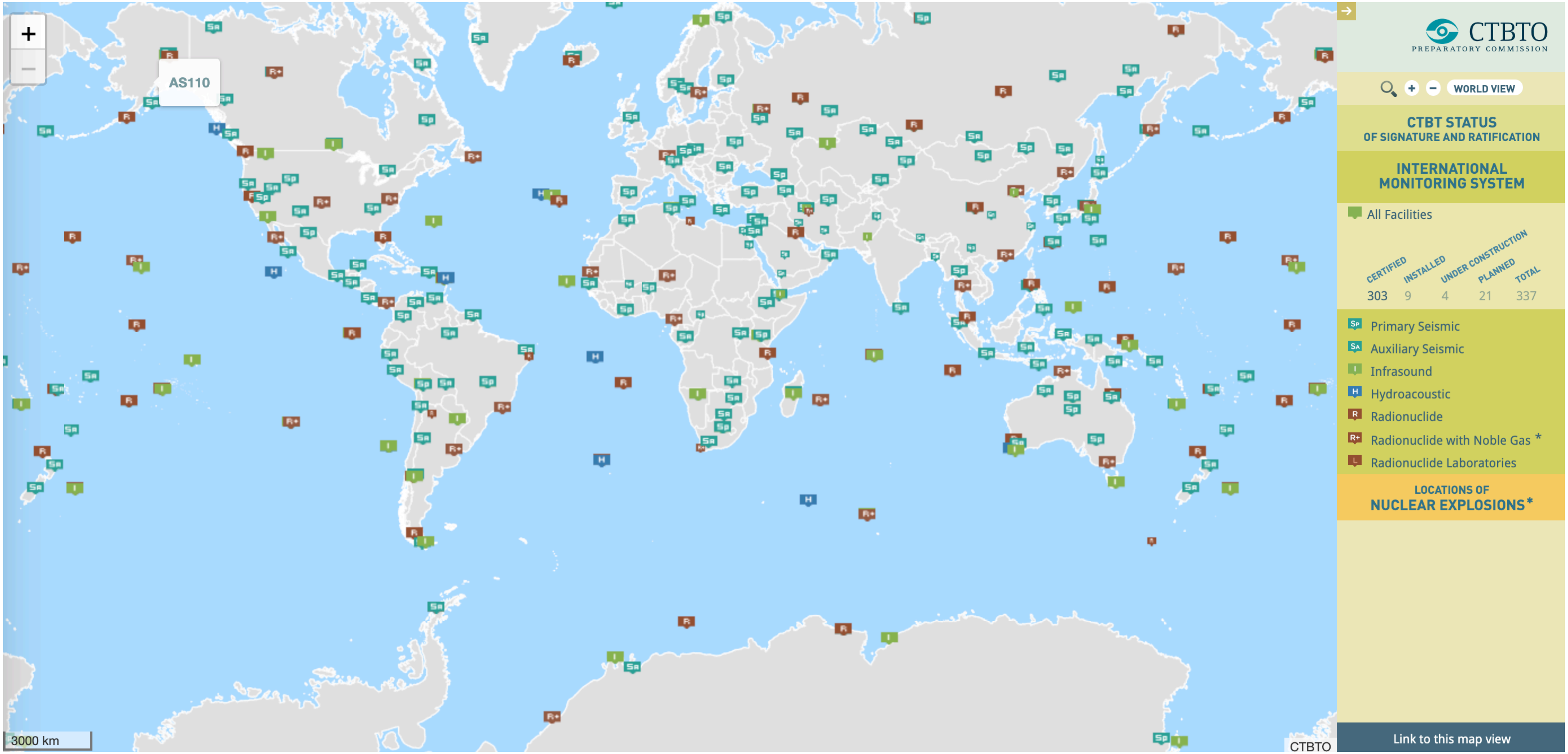

AS110
3000 km
CTBTO
CTBTO
PREPARATORY COMMISSION
WORLD VIEW
CTBT STATUS
OF SIGNATURE AND RATIFICATION
INTERNATIONAL MONITORING SYSTEM
All Facilities
CERTIFIED 303
INSTALLED 9
UNDER CONSTRUCTION 4
PLANNED 21
TOTAL 337
Primary Seismic
Auxiliary Seismic
Infrasound
Hydroacoustic
Radionuclide
Radionuclide with Noble Gas *
Radionuclide Laboratories
LOCATIONS OF
NUCLEAR EXPLOSIONS*
Link to this map view

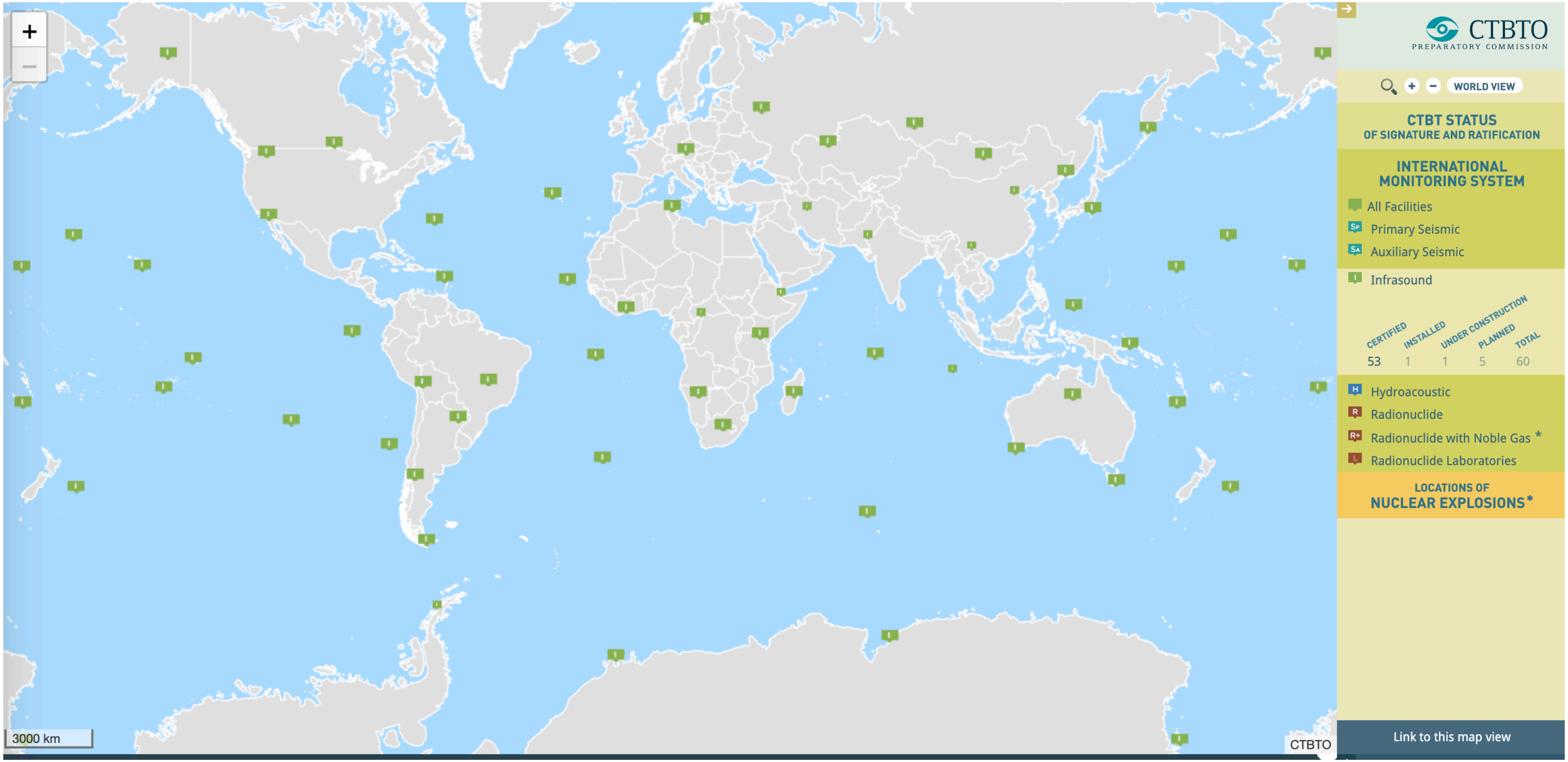

3000 km
CTBTO
CTBTO
PREPARATORY COMMISSION
WORLD VIEW
CTBT STATUS
OF SIGNATURE AND RATIFICATION
INTERNATIONAL MONITORING SYSTEM
All Facilities
Primary Seismic
Auxiliary Seismic
Infrasound
CERTIFIED
INSTALLED
UNDER CONSTRUCTION
PLANNED
TOTAL
53
1
1
5
60
Hydroacoustic
Radionuclide
Radionuclide with Noble Gas *
Radionuclide Laboratories
LOCATIONS OF
NUCLEAR EXPLOSIONS*
Link to this map view